

# DEUTSCHES ELEKTRONEN - SYNCHROTRON **DESY**

Interner Bericht

H-14

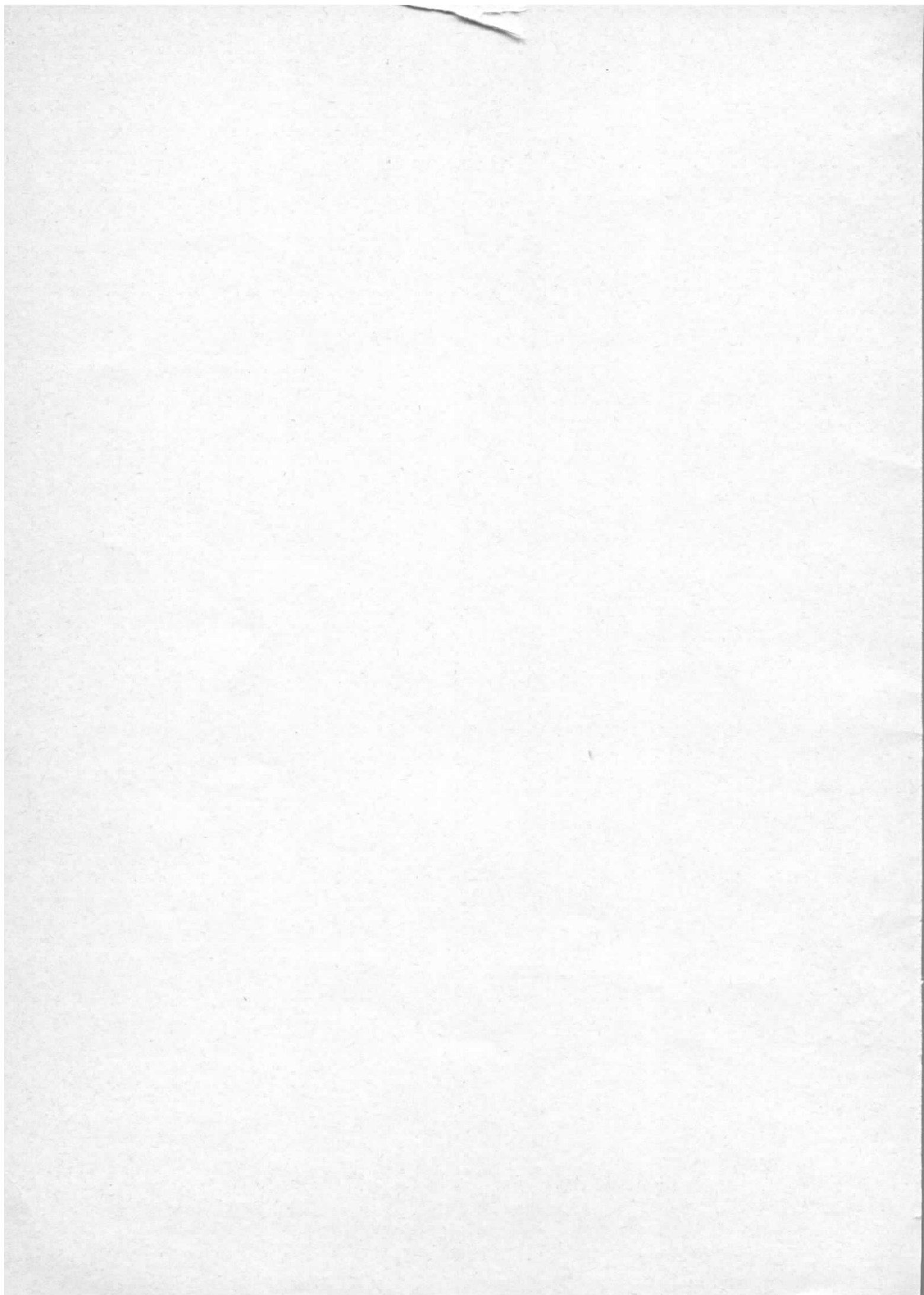
November 1966

A POSITRON FOCUSING SYSTEM  
FOR  
LINEAR ACCELERATORS

by

H. Wiedemann

2 HAMBURG 52 · NOTKESTIEG 1

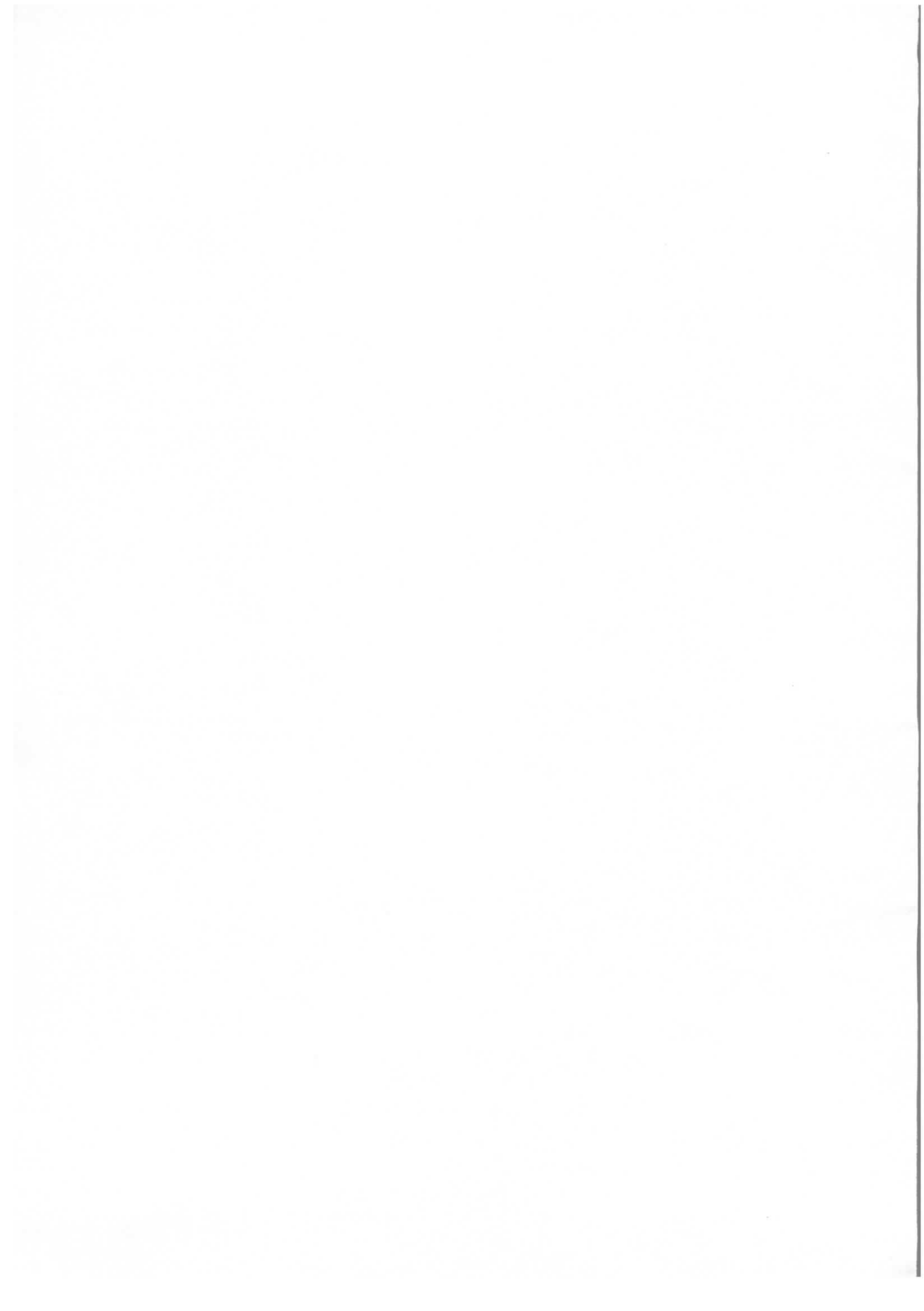


H. Wiedemann

Hamburg, den 10.11.66

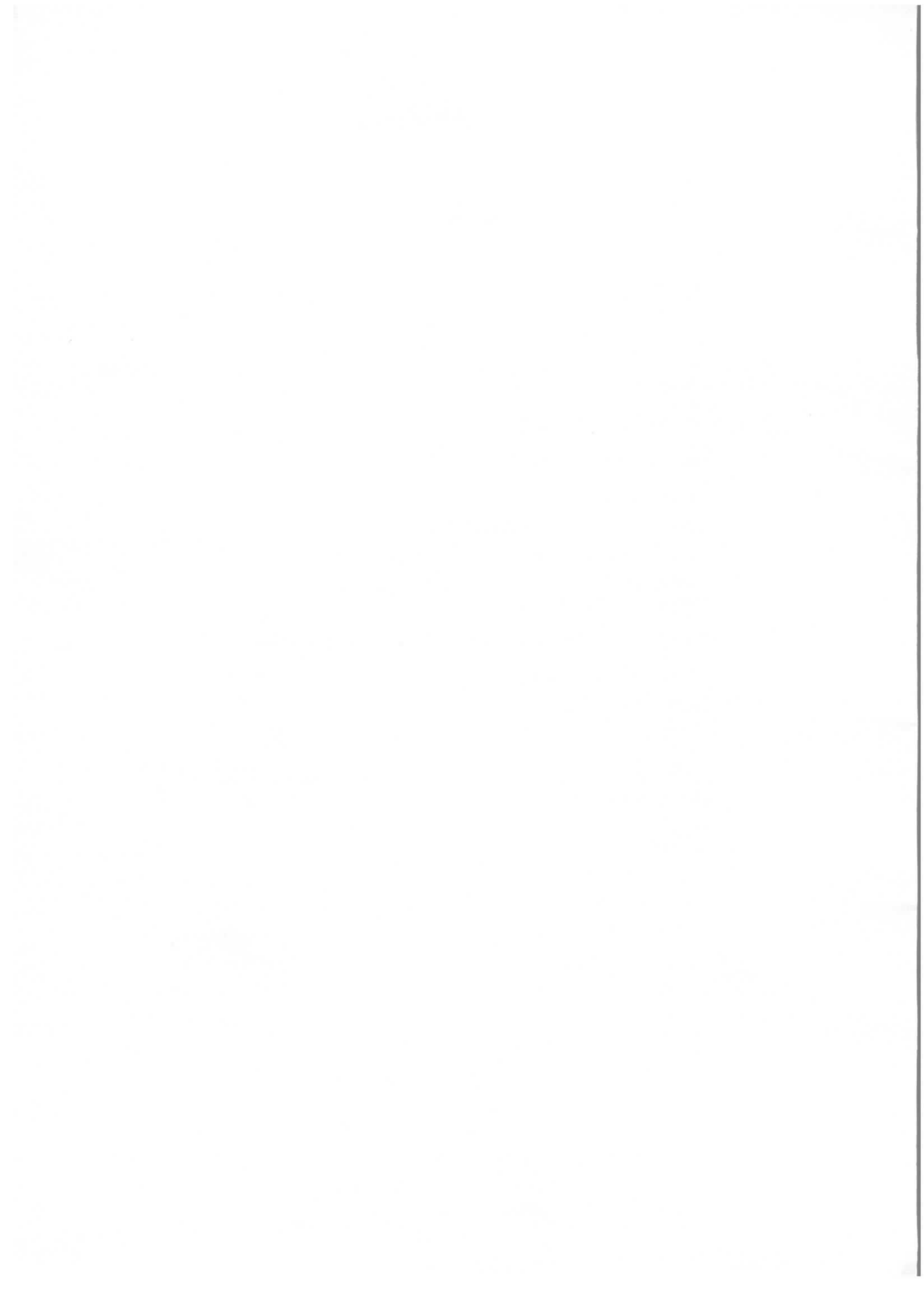
DESY H 14

A POSITRON FOCUSING SYSTEM  
FOR  
LINEAR ACCELERATORS



## I n d e x

Introduction	1
I. The converter target	1
II. Initial positron focusing	3
Positron intensities	3
Optics of the positron horn	4
Technical design of the positron horn	8
Mechanical forces due to the pulsed magnetic field	9
III. Positron focusing in the linear accelerator	10
Solenoid and quadrupole focusing	10
FODO channel	15
Solenoid in the first two positron linac sections	16
FODO-channel in the remaining 5 positron linac sections	19
Literature	21



## Introduction

The new 300 MeV linear accelerator as an injector for DESY is planned to accelerate both electrons and positrons.

In this paper, a target and a focusing system is described which yields a high intensity analysed positron current of a few 2 mA at the end of the linac. The accelerator gives an electron pulse power of more than 50 MW on the converter target, and accelerates the positrons in seven following sections to 360 MeV.

This paper essentially is a translation of the DESY-note H9, August 1965. However, new calculations and informations on the positron horn have been included in addition.

### I. Converter Target

For positron production a converter target is needed, which withstands an electron pulse power of 50 MW and 3 to 7 kW average for a long time.

The converter targets built and proposed so far consist of a moving tungsten annulus. This metal combines a high Z with a high melting point and a rather good heat conduction. But like all other solid target materials, tungsten has the disadvantage that the target has to be rapidly moved with its cooling system in the high vacuum in order to avoid too high temperatures. Besides this, tungsten is very brittle and will be mechanically destroyed by the point heating.

Both disadvantages can be avoided by a fluid metal target in which the heat will be transported by forced convection and the mechanical destruction of the housing may be strongly reduced

by taking a low Z metal (e.g. steel). The following calculations assume Wood's metal as converter target.

For simplicity we assume that the thermal energy deposited on the target by the electron pulse is equal to the lost ionisation energy of the electrons. The calculation results in:

$$(1) \quad - \frac{\Delta E}{\Delta x} = 17 \frac{\text{MeV}}{\text{cm}}$$

As we show in a later section, the optimum target-thickness is about 1.5 radiation length, or for Wood's metal  $l = 0.75$  cm.

The deposited thermal energy is

$$(2) \quad \Delta Q = 0.9 \text{ cal/pulse}$$

for a pulse duration of 1  $\mu\text{sec}$ . This corresponds to a temperature rise of

$$(3) \quad \Delta T = \frac{\Delta Q}{\rho \cdot V \cdot c} = 137^\circ\text{C}$$

(target volume  $V = \pi \frac{d^2}{4} \cdot l$ ;  $d = 2$  mm) if the effective target cross section is taken equal to the electron beam cross section.

This temperature rise per pulse does not appear too large for a steel target housing.

The Wood's metal will be made fluid by electric heating and will be pumped by an electromagnetic pump without rotating elements.

## II. Initial Positron Focusing

### 1. Positron intensities

There are results of two experiments which allow to calculate the yield of the positron conversion. In Orsay, T.L. Aggson and L. Burnot (AG62) measured positron intensities in the foreward direction ( $\delta = \pm 2^\circ$ ) for various positron energies and various electron energies between 55 MeV and 220 MeV. Since we like to focus the positrons over a wide solid angle, we cannot take quantitative results from these measurements. Qualitatively, the measurement yields a broad intensity maximum for positron energies between 5 and 10 MeV for all electron energies. A second important result for us is the optimal target thickness which is about 1.5 radiation lengths independent of the electron energy.

The most important source for our intensity calculations are measurements of De Staebler (STAE 63) in Stanford. He measured the angular distribution of positrons at various positron energies. The electron energy was 1 GeV. De Staebler also found an intensity maximum for positron energies between 5 and 10 MeV (Fig. 1).

As for the absolute values, De Staebler interprets them as low value limits. He assumes that by scattering mainly of the low energy positrons in the spectrometer windows, about 30 % of the positrons are lost. In spite of this, we take the figures of De Staebler's report for our further calculations.

Integration over the angle of De Staebler's figures gives positron intensities for various solid angles (Fig. 2) for an electron energy of 1 GeV and positron energies between 5 and 10 MeV.

Our new linear accelerator gives at the converter an electron pulse current of 322 mA at 177 MeV, i.e. a pulse power of  $P = 57$  MW. The positrons are accelerated in the second part of the linear accelerator to 360 MeV. For this power, for an initial energy width of  $\Delta E_+ = 3,6$  MeV for the positrons, corresponding to a relative energy range of 1 % at the end of the linac and a solid angle given by  $\delta = 40^\circ$  one gets a positron current of

$$(4) \quad J_+ = \left( \frac{1}{E_0} \frac{\Delta n_+}{\Delta E_+} \right) P_- \cdot \Delta E_+ = 15 \text{ mA}$$

This is the lower limit; the real positron current may be up to 50 % higher. Supposing that the focusing efficiency of the positron horn is about 50 % and assuming that one third of the positrons (Am 63) captured in the linac will remain in an energy range of 1 % during acceleration this yields in a positron pulse current of

$$(5) \quad J_+ = 2,5 \text{ mA}$$

which can be injected in the synchrotron. This current corresponds to an effective converting efficiency of

$$(6) \quad \eta_+ = 0,05 \frac{e^+}{e^- \cdot \text{GeV}}$$

into an energy range of  $\Delta E_+/E_+ = \pm 0,5$  % and into an emittance of  $1,6 \text{ } \mu\text{radcm}$  (see following section)

## 2. Optics of the positron horn

The design aim of the positron focusing system is to focus positrons of 6 MeV and production angles up to  $40 - 45$  degrees into an emittance area of  $100 \text{ } \mu\text{radcm}$ , which gives at 360 MeV an emittance of  $1,67 \text{ } \mu\text{radcm}$  corresponding to the acceptance of the synchrotron.

In the positron linear accelerators built and proposed so far the positron target is immersed in a strong solenoid field (Am 63, Mi 65) which yields a parallel positron beam from a point source. To focus positrons up to a production angle of  $14^\circ$  a magnetic field strength of 17,7 kGauss is needed. To go to even higher magnetic fields seems to be technically difficult.

In order to focus positrons over a larger angle one has to use a magnetic field normal to the positron trajectories, which can be produced by an axial electric current used in the Neutrino-experiment. This is done at CERN by the so called "Magnetic Horn" (ME 61, ME 62, AS 65). In Novosibirsk (BU 63) they use a parabolic lens which is essentially a "horn" to focus a 700 MeV electron beam on a target and to make the divergent positron beam parallel. In our case, we cannot use such a parabolic lens because the efficiency is too small. Therefore, we propose a horn which is similar to the CERN-type (Fig. 3).

For the particle trajectories in a coaxial magnetic field one gets (e.g. from the equation (19)) the differential equations in polar coordinates  $\{r, \phi, z\}$  :

$$r'' - r\phi'^2 + \epsilon \frac{z'}{r} = 0$$

$$\frac{d}{ds} (r^2 \phi') = 0$$

$$z'' - \epsilon \frac{r'}{r} = 0$$

$$\epsilon = \frac{2eI}{cE}$$

For focusing the positrons on a point, one has to shape the horn such that each particle escape the magnetic field when the tangent of its trajectory aims at this focus. However, this is only possible for monoenergetic particles from a

ring source. To "focus" particles of an energy range of some MeV originating from an extended source, one has to give the horn such a form that as many positrons as possible aim at a spot of about 2 cm diameter corresponding to the aperture of the linear accelerator.

For this purpose the differential equations (8) have been written as follows:

$$(8) \quad r^2 \phi' = \frac{\rho^2 \phi_0}{c} = \alpha$$

$\rho$  : radius of the target

$m\rho^2 \phi_0$  : angular momentum

With (8) eq. (7) reduces to

$$(9) \quad r^3 r'' - \alpha^2 + \epsilon z' r^2 = 0$$

$$z'' r - \epsilon r' = 0$$

These equations have been solved on the analog computer for various initial conditions  $\{r_0, \phi_0, z_0\}$ .

The magnetic field has been chosen such that particles of 6 MeV and an initial angle of 40 degrees are bent to the forward direction within about 1 cm distance from the axis. This high field is necessary to avoid too large differences in path length and can be realized with a pulse current of 15000 Amperes.

Typical particle trajectories for different initial conditions are shown in Figures 4 and 5. From a large number of calculated trajectories a favourable horn-profile as shown in Fig. 6 has been derived. This horn-profile should be a good compromise between the ideal profiles for different energies and source points.

With this horn profile (Fig. 6) many particle trajectories have been calculated to get the emittance area of the horn (Fig. 7) at  $z = 8$  cm. This plane has been found to have the highest particle density. The ellipses shown in Fig. 7 give the acceptance of the downstream solenoid for different energies (see later sections).

The Figure 7 shows that with the positron horn positrons can be captured over a large solid angle and a broad energy range. The energy spectrum for these captured positrons is shown in Fig. 8. For comparison the energy spectrum accepted by a solenoid is given, for which Amman (Am 63) obtains the equation (see Fig. 8a):

$$(10) \quad \left(\frac{\delta}{\delta_0}\right)^2 = \frac{(V_0/V)^2}{(H_1/H_2)^2 \cos\left(\frac{\pi}{2} \frac{V_0}{V}\right) + \sin\left(\frac{\pi}{2} \frac{V_0}{V}\right)}$$

$$(V_0 = 10 \text{ MeV}, H_1 = 17,7 \text{ k}\Gamma, H_2 = 4 \text{ k}\Gamma, \delta_0 = 14^\circ)$$

The calculation shows that the positron horn does not only yield an essentially higher positron intensity, but also a broader energy spectrum, which is advantageous for the acceleration in a linear accelerator. There, the single positron bunches are broadened (e.g. by phase errors and field inhomogenities) so that only about 30 % (Am 63) of the initial positron intensity remains in an energy band of  $\pm 0.5$  %. This percentage increases if the energy band of the positrons is large.

Another advantage connected with the positron horn are the small phase differences between particles on different trajectories. Fig. 9 shows these phase differences for different energies and initial angles. All positrons between 4 and 8 MeV are within a phase angle of  $\pm 4$  degree.

The primary electrons have the same phase spread, so that the positrons are within  $\pm 8^\circ$  that means within an energy gap of  $\pm 0.5\%$  for an ideal 3000 mc linac.

### 3. Technical design of the positron horn

Because of the very low positron energy, we cannot apply the lens types used at CERN and Novosibirsk; we have to approximate the coaxial magnetic field by a few thin current carrying wires as already shown in Fig. 3.

The actual field as shown in figures 10 and 11 was obtained by digital computer calculation. The field is very distorted in the vicinity of the wires. However, the azimuthal deflection of particles due to radial field components is not serious (less than 35 mrad). The calculation of the positron current in eq. (4) is based on an effective horn transparency of only 70 %; that means the vicinity of the wires has been neglected for intensity calculations.

The positron horn is connected over a spark gap to a delay line. The pulse charge is 0.06 Asec, 50 times per sec. The ohmic losses rapidly rise the temperature of the wires so that water cooling at the ends of the horn is needed. The material of the horn wires is the silver alloy Argodur 32. This alloy has the high and constant tensile strength of 53 kp/mm up to a temperature of 650°C. This material seems to be the best for our purpose and will withstand the magnetic forces also at high temperatures. The electrical resistance is about 13 % higher compared with pure silver.

The energy deposited on 1 cm of wire length is:

$$(11) \quad \Delta Q = 1,0 \cdot 10^{-3} \text{ cal/cm} \cdot \text{pulse}$$

For a wire length of 4.5 cm this gives a total energy of 0.009 cal which has to be transported by heat conduction to the ends of the horn within 20 msec. For silver this results in a temperature gradient of

$$(12) \quad \Delta T = 160^{\circ}\text{C/cm}$$

The temperature in the middle of the wire therefore is  $360^{\circ}\text{C}$ . This is an upper limit because radiation has been neglected.

#### 4. Mechanical forces by the pulsed magnetic field

We regard a wire which is supported only at its ends. For such a wire the eigenfrequencies are:

$$(13) \quad \omega_n = \alpha_n^2 c_w \frac{h}{\sqrt{12}}$$

$h$ : height of the wire (here 1 mm)

$c_w$ :  $E/\rho$

$\alpha_n$ : eigenvalues of the frequency equation  $1 - \cos l \cdot \cosh l = 0$   
The first three eigenvalues are:

$$(14) \quad \begin{aligned} \alpha_1 l &= 4,7300 \\ \alpha_2 l &= 7,8532 \\ \alpha_3 l &= 10,9956 \end{aligned}$$

$h = 1 \text{ mm}$ ,  $l = 4,5 \text{ cm}$ ,  $E = 8000 \text{ kp/cm}^2$  (Argodur 32)  
 $\rho = 10,5 \text{ g/cm}^3$  yields for the three first eigenoscillations:

$$(15) \quad \begin{aligned} \omega_1 &= 7,6 \cdot 10^3 \text{ sec}^{-1} \\ \omega_2 &= 21,2 \cdot 10^3 \text{ sec}^{-1} \\ \omega_3 &= 35,5 \cdot 10^3 \text{ sec}^{-1} \end{aligned}$$

These frequencies are very small compared with the pulse frequency of  $\omega_p = 1,6 \cdot 10^6 \text{ sec}^{-1}$  (2  $\mu\text{sec}$  pulse length) that means both the pulse frequency and the pulse sequence frequency of  $\omega_o = 314 \text{ sec}^{-1}$  are far away from the resonance frequencies. The wires are not excited to considerable oscillation. A calculation yields a maximum oscillation amplitude of  $10^{-5} \text{ cm}$ . That means that, in spite of the high current in a high magnetic field no additional supports besides the end supports are needed.

### III. Positron focusing in the linear accelerator

#### 1. Solenoid and quadrupole focusing

The positrons will be accelerated up to  $\hat{E} = 360 \text{ MeV}$  in seven sections following the converter and will then be injected into the DESY synchrotron. The acceptance of the synchrotron is  $\epsilon = 2 \text{ mradcm}$ . According to Liouville's theorem we get a useful emittance of the positron horn of

$$(16) \quad \pi r r' = 2 \pi \frac{\hat{E}}{E_o} = \pi \frac{720}{E_o} r \text{ mradcm}$$

i.e. with  $E_o = 6 \text{ MeV}$  and  $r = 1 \text{ cm}$ , a positron divergence up to  $120 \text{ mrad}$  can be accepted. Safely, we have used  $r' = 100 \text{ mrad}$  in our calculation (see Fig. 7).

This corresponding emittance of  $100 \text{ mradcm}$  is to be transformed to the end of the linac with the lowest possible focusing power.

There are two essential methods for positron focusing:

- a) Focusing with the aid of an axial solenoidal magnetic field.

b) Focusing with magnetic quadrupole lenses.

The efficiency of the quadrupole focusing is higher than that of a solenoid. While the pure solenoid magnetic field has to be maintained over the whole accelerator length, the spacing between the single lenses in quadrupole focusing increases adiabatically. This difference is more and more observable with higher particle momentum. However we will see that there are cases in which only solenoids can be used.

The particles are assumed to be highly relativistic ( $\gamma \gg m_0 c^2$ ).

The general equations of motion in a Cartesian coordinate system are

$$(17) \quad \frac{d}{dt} (m\vec{v}) = e\vec{E} + \frac{e}{c} \cdot [\vec{v} \times \vec{B}]$$

Transforming to the particle trajectories by inserting

$$(18) \quad \frac{d}{dt} = \frac{ds}{dt} \frac{d}{ds} = c \cdot \frac{d}{dt}$$

one gets with (17)

$$(19) \quad \vec{r}'' + \frac{(mc^2)'}{mc^2} \vec{r}' - \frac{e\vec{E}}{mc^2} - \frac{e}{mc^2} [\vec{r}' \times \vec{B}] = 0 \quad \vec{r}(x, z, s)$$

Primes are derivatives with respect to the trajectory lengths  $s$ .

With

$$(20) \quad mc^2 = m_0 c^2 (\alpha s + \gamma_0) = m_0 c^2 \cdot \alpha \cdot (s + \lambda)$$

$\gamma_0$ : initial energy at the entrance in the focusing system

$\alpha$ : energy gradient (MeV/m/ $m_0 c^2$ )

and

$$(21) \quad e |\vec{E}| = m_0 c^2 \cdot \alpha$$

we get

$$(22) \quad \vec{r}'' + \frac{1}{s + \gamma} \vec{r}' - \frac{e \vec{E}}{\alpha(s + \gamma)m_0 c^2} - \frac{e}{\alpha(s + \gamma)m_0 c^2} (\vec{r}' \times \vec{B}) = 0$$

To simplify the differential equation system (22) we change to the system  $\{x, z, \tau\}$  of the accelerated particle:

$$(23) \quad \gamma_0 ds = \gamma d\tau$$

$$(24) \quad \frac{d^2}{d\tau^2} \vec{r} - \frac{\gamma \cdot e \vec{E}}{\gamma_0 \cdot m_0 c^2} - \frac{e}{\gamma_0 \cdot m_0 c^2} \frac{d}{d\tau} (\vec{r} \times \vec{B}) = 0$$

We will use this system of differential equations for the two types of magnetic fields:

a) Solenoid focusing , characterized by

$$\begin{aligned} \vec{B} & (0, 0, B) \\ \vec{E} & (0, 0, E), \end{aligned}$$

$$(24) \text{ yields } \ddot{z} - \frac{e}{m_0 c^2 \cdot \gamma_0} \dot{x} B = 0$$

$$(25) \quad \ddot{x} + \frac{e}{m_0 c^2 \cdot \gamma_0} \dot{z} B = 0$$

(Points are derivatives with respect to  $\tau$ )

Separation of the variables yields with (20) and (21)

$$(26) \quad \begin{aligned} \ddot{z} + \left(\frac{B}{\lambda E}\right)^2 \dot{z} &= 0 \\ \ddot{x} + \left(\frac{B}{\lambda E}\right)^2 \dot{x} &= 0 \end{aligned}$$

A main solution for (26) is

$$(27) \quad y = A \cdot \cos \frac{B}{\lambda E} \tau$$

Going back again to the laboratory system by  $\tau = \lambda \log \frac{s+\lambda}{\lambda}$  one gets

$$(28) \quad y = A \cdot \cos \left(\frac{B}{E} \log \frac{s+\lambda}{\lambda}\right)$$

and

$$(29) \quad y' = -A \frac{B}{E} \cdot \frac{1}{s+\lambda} \sin \left(\frac{B}{\lambda E} \log \frac{s+\lambda}{\lambda}\right)$$

The particles oscillate undamped in both coordinates with increasing wave length. That means in a solenoid field the acceleration reduces the beam divergence only. As the beam cross section and the radial particle momentum stay constant, the magnetic field has to be carried in its full strength up to the end of the accelerator.

b) Focusing with quadrupoles

With  $\vec{B} (B_z, B_x, 0)$

(24) yields

$$(30) \quad \begin{aligned} \ddot{z} + \frac{e}{m_0 c^2 \gamma_0} \dot{s} B_x &= 0 \\ \ddot{x} - \frac{e}{m_0 c^2 \gamma_0} \dot{s} B_z &= 0 \end{aligned}$$

These equations are simplified by (23)

$$(31) \quad B_x = gz; \quad B_z = gx; \quad g = g(s)$$

giving

$$(32) \quad \ddot{y} \pm \frac{e \cdot \gamma}{m_0 c^2 \cdot \gamma_0} g \cdot y = 0$$

(y is taken for x and z)

For thin lenses (32) further reduces by introducing the quantity Q

$$(33) \quad Q = \frac{\delta B_x}{\delta z} ds = g \cdot L_{Q_0}$$

where  $L_{Q_0}$  is the quadrupole length in the laboratory system. For a relativistic particle the quadrupole length is reduced to

$$(34) \quad L_Q = \frac{\gamma_0}{\gamma} L_{Q_0}$$

where  $L_Q$  is the quadrupole length in the particle system.

(33) and (34) gives

$$g = \frac{Q}{L_{Q_0}} = \frac{\gamma_0}{\gamma} \frac{Q}{L_Q}$$

To get a periodic solution for (32) the product  $\gamma \cdot g$  has to be constant. That means  $Q/L_Q = g_0$  and

$$(36) \quad g = \frac{\gamma_0}{\gamma} g_0$$

With the lens strength  $k_0$ :

$$(34) \quad k_0 = \frac{e}{p_0} g_0 = \frac{ec}{m_0 c^2 \cdot \gamma_0} g_0$$

we get

$$(38) \quad \ddot{y} \pm k_0 y = 0$$

Thus, one has a motion similar to that of unaccelerated particle in a periodic quadrupole channel if one keeps the quadrupole strength  $k_0$  and length  $L_{Q_0}$  constant and monotonically increases the spacing between quadrupole centers according to eq. (23). This shows the advantage of the quadrupole focusing for long accelerators.

## 2. FODO-Channel

A suitable quadrupole focusing system for the positrons in a linear accelerator is the periodic FODO-channel.

For the determination of the optimum quadrupole arrangement Steffen (STE 65) gave the following formulae:

$$(39) \quad \phi = 1 \sqrt{k}$$

$$(40) \quad m^2 = \frac{1 + \tanh\phi(\tan\phi + \frac{L}{l}\phi)}{1 - \tanh\phi(\tanh\phi + \frac{L}{l}\phi)}$$

$$(41) \quad \epsilon^2 = \frac{R^4}{l^2} \frac{m^2}{(1+m^2)^2} \frac{[\tan\phi(\tanh\phi + \frac{L}{l}\phi) - 1] \phi^2}{1 + \tanh\phi(\tan\phi + \frac{L}{l}\phi)}$$

k: lens strength

m: beat factor

$\epsilon$ : acceptance of the FODO-channel

R: minimum radius of the irishole

l: lens length

L: distance between lenses

In order to find the optimum parameter for a given acceptance and lens length, we calculated on the digital computer the functions  $\epsilon_{\max}(L,l)$ ,  $m_{\text{opt}}(L,l)$  and  $k_{\text{opt}}(L,l)$  (see Fig. 12). The calculation yielded a constant beat factor  $m_{\text{opt}} = 2,3$ . The maximum acceptance increases with decreasing  $L$  and  $l$ . This shows the limitation of quadrupole focusing. In order to get a proper quadrupole field, the quadrupole length should be about twice as big as the aperture diameter. Since in the linac the quadrupole aperture has to include the accelerating structure, the diameter must be of the order of 15 cm and, accordingly, the lens length must be at least 25 to 30 cm. Because of the quadrupole coil ends the distance  $L$  has to be larger than 15 cm. This requirement restricts the application of quadrupole focusing, and figure 12 shows that it is impossible to start with the FODO-channel directly behind the positron horn. Therefore, we are obliged to focus the positrons in the first two accelerator sections following the converter by means of a strong solenoid field.

### 3. Solenoid field in the first two positron linac sections

The positrons spiral in the solenoid field with a radius given by

$$(42) \quad \rho = \frac{E_0 r_0'}{eB}$$

$E_r/c$ : radial momentum

$E_0$ : initial energy

$B$ : solenoid field strength

For  $\rho \leq 0,5$  cm and  $E_0 = 6,0$  MeV and  $r_0' = 100$  mrad we need a magnetic field of 4Kr.

The phase area  $F = \pi r r'$  decreases with increasing energy and we can change to quadrupole focusing the earlier the faster the particles are accelerated.

With a klystron power of 20 MW each the positrons reach an energy of 114 MeV after the first two accelerator sections. At this energy the phase area has reduced from 100  $\pi$ radcm to 5,26  $\pi$ radcm.

Thus the emittance is small enough to change to quadrupole focusing.

#### Acceptance and Emittance of the Solenoid

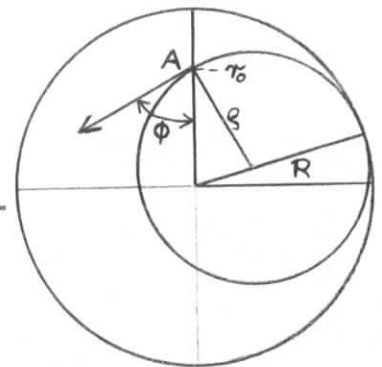
For a positron entering the solenoid fringe field at A (see Figure) with the angle  $\phi$  to the axis the maximum radius of the spiral in the solenoid field is given by the radius  $\rho$  resulting from

$$(43) \quad (r_0 - \rho \sin \phi)^2 + \rho^2 \cos^2 \phi = (R - \rho)^2$$

or

$$(44) \quad 2\rho_{\max} = \frac{R^2 - r_0^2}{R - r_0 \sin \phi}$$

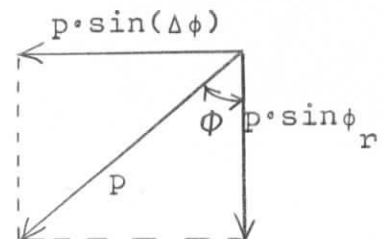
solenoid-aperture



In the fringe field the positrons get an azimuthal momentum  $\Delta p = p_0 \sin \Delta \phi$  while the radial momentum  $p_r = p_0 \sin \phi_r$  remains constant.

The particle momentum normal to the magnetic field lines is given by

$$(45) \quad p_{\perp} = p_0 \sqrt{\sin^2 \phi_r + \sin^2 \Delta \phi}$$



With (46) 
$$\frac{1}{\rho_{\max}} = \frac{eB}{cp_{\perp}}$$

and (44) this yields

(47) 
$$p_{\perp} = \frac{r_0}{R} p_0 \sin \Delta\phi + \frac{R^2 - r_0^2}{R} \frac{eB_0}{c}$$

The approximation  $\sin \Delta\phi \approx \Delta\phi$  and  $\sin \phi_r \approx \phi_r$  leads with (45) to

(48) 
$$\phi_r = \pm \frac{1}{2} \frac{R}{R_0} \sqrt{1 - \left(\frac{r_0}{R}\right)^2}$$

where

$$R_0 = \frac{cp}{eB} \text{ and } \Delta\phi = \frac{1}{2} \frac{eB}{cp} r \text{ (Am 63)}$$

For  $B = 4$  kG and  $R = 1$  cm we get

(48a) 
$$\phi_r < \pm \frac{0,6}{p_0 (\text{MeV}/c)} \sqrt{1 - r_0^2}$$

The solenoid acceptance therefore is

(49) 
$$\alpha_{\text{sol}} = \frac{0,6}{p_0} \cdot R\pi = \frac{600 \cdot \pi}{p_0 (\text{MeV}/c)} \text{ mradcm.}$$

The emittance at the end of the solenoid is within a few per cent the same for all energies because of the adiabatic damping during acceleration. The beam cross section remains constant while the divergence decreases with increasing energy. With  $E_1$  being the positron energy at the end of the solenoids, the emittance for all initial momenta is given by

(50) 
$$\epsilon_{\text{sol}} = \frac{600 \pi}{\frac{E_1}{c} (\text{MeV}/c)} \text{ mradcm}$$

In our case the emittance of the solenoid for  $E_1 = 114$  MeV is

$$(50a) \quad \epsilon_{\text{sol}} = 5,26 \text{ } \pi\text{mradcm}$$

This emittance is small enough to be matched into the FODO-channel which is done by a quadrupole doublet.

#### 4. FODO-channel in the remaining 5 positron linac sections

For further focusing following a FODO-channel is used which has the following parameters (see Fig. 12)

$$\begin{aligned} \epsilon &= 5,28 \text{ mradcm} \\ L &= 30 \text{ cm} \\ 2l &= 30 \text{ cm} \\ K &= 9,86 \text{ m}^{-2} \\ g &= 374 \text{ G/cm} \end{aligned}$$

With a useful iris diameter  $2R = 2,2$  cm of the accelerating structure and a beat factor of 2,3 we get a rectangular beam cross section with half sides  $a = 1,01$  cm and  $b = 0.43$  cm.

The free distances  $L$  have to be transformed to get the quadrupole separations in the laboratory system.

The distance  $L_n$  of the center of the  $n$ th quadrupole from the plane  $s = 0$  is given by

$$(51) \quad L_n = \lambda(e^{nL'/\lambda} - 1)$$

With an acceleration  $\alpha = 0,18 m_0 c^2/1/\text{cm}$ ,  $\gamma_0 = 224$  and  $L' = L + 2l = 60$  cm one needs 25 quadrupoles to focus the positrons up to an energy of 360 MeV.

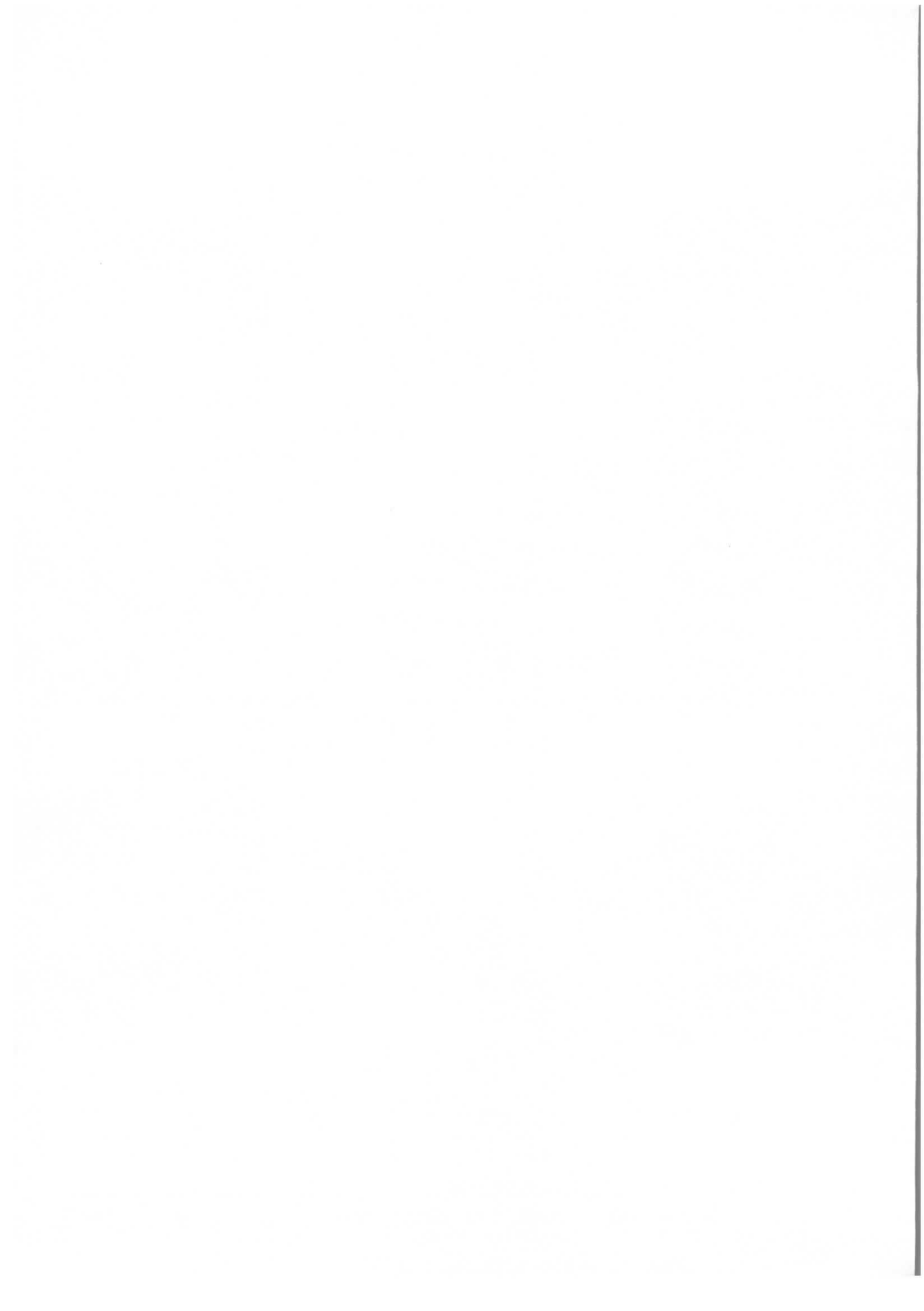
Here, however, detailed calculations showed that the transformation (23) is not exactly correct. In the derivation of eq. (38) we used in the coefficient a "thin lens" approximation by the substitution (35). One gets the precise FODO-structure by reducing the beam phase area according to the increase of energy, taking from Fig. 13 the corresponding quadrupole distances and with these from Fig. 14 the lens strengths. In Fig. 15 the corrected quadrupole distances and lens strengths are compared with those calculated with eq. (51). One can see that the lens strengths and lens separation have to be slightly smaller.

#### Acknowledgement

I wish to acknowledge many useful discussions with K.G. Steffen in preparing this work. Also I wish to thank Miss Borchardt for programming the particle trajectories in the positron horn at the analog computer, Mr. Haupt for the calculation of the magnetic field in the positron horn at the digital computer and Mr. Knaut for the drawing. Last not least I thank Miss Möhring for her assistance in translating this report.

Literature

- AG 62 : T.L. Aggson - L. Burnot, LAL 27, Orsay 1962  
AM 63 : F. Amman - R. Andreani LNF - 63/46  
AS 65 : A. Asner, CERN 65 - 17  
BU 63 : G.I. Budker, Conference Report, DUBNA 1963  
ME 61 : S. van der Meer, CERN 61-7  
ME 62 : S. van der Meer, CERN 62 - 16  
Mi 65 : M.C. Crowley-Milling EL/TM/27  
STAE 63: De Staebler SLAC-TN-65-23  
STE 65: K.G. Steffen, High Energy Beam Optics, I. Wiley 65



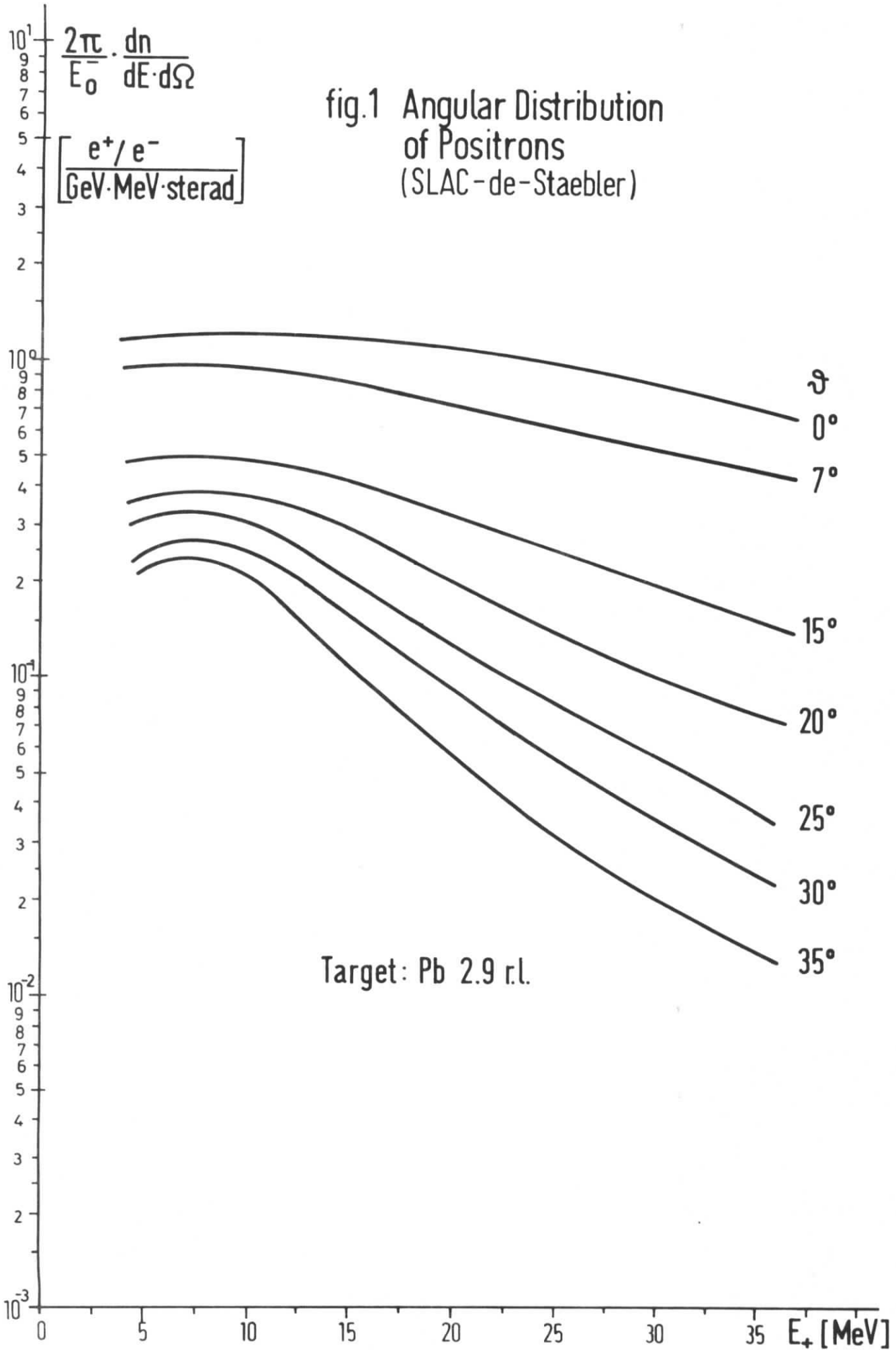
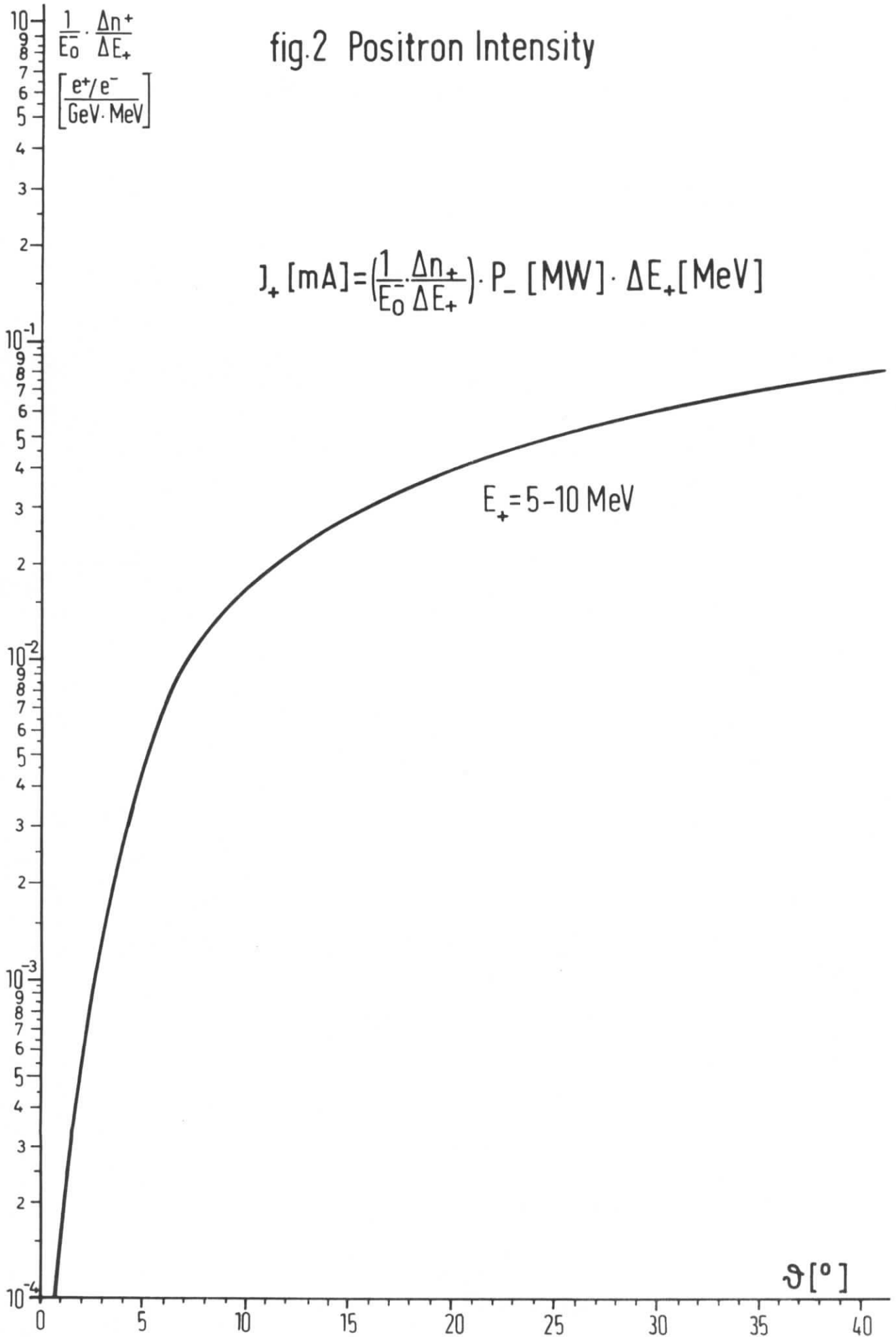
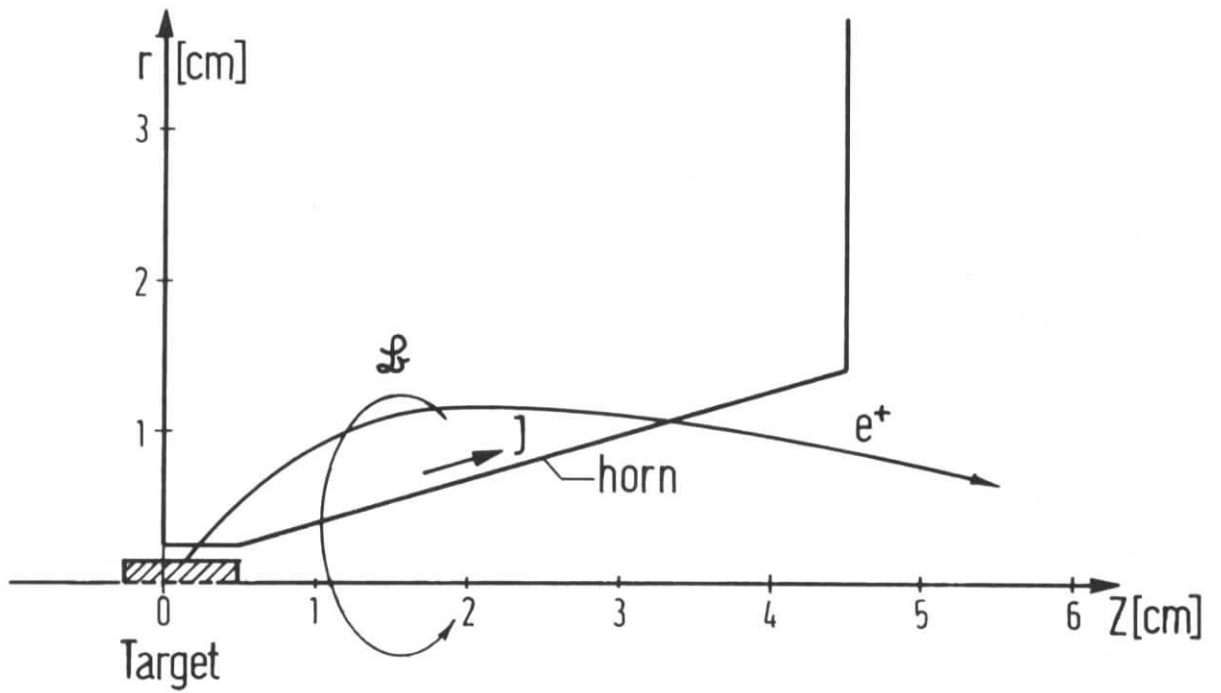


fig.2 Positron Intensity



# Positron Horn (schematic)



## A Horn-Cross-Section

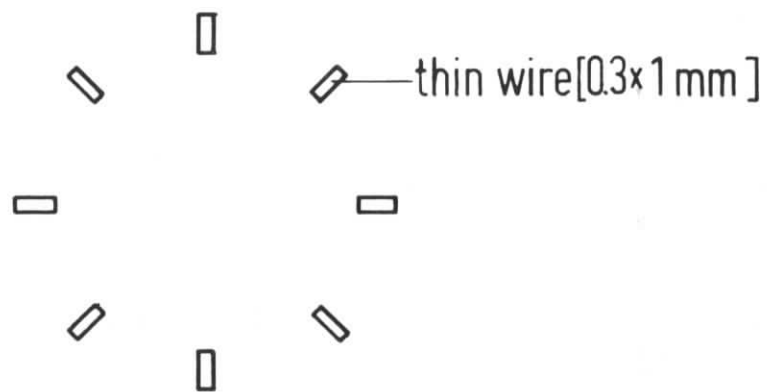


fig.3

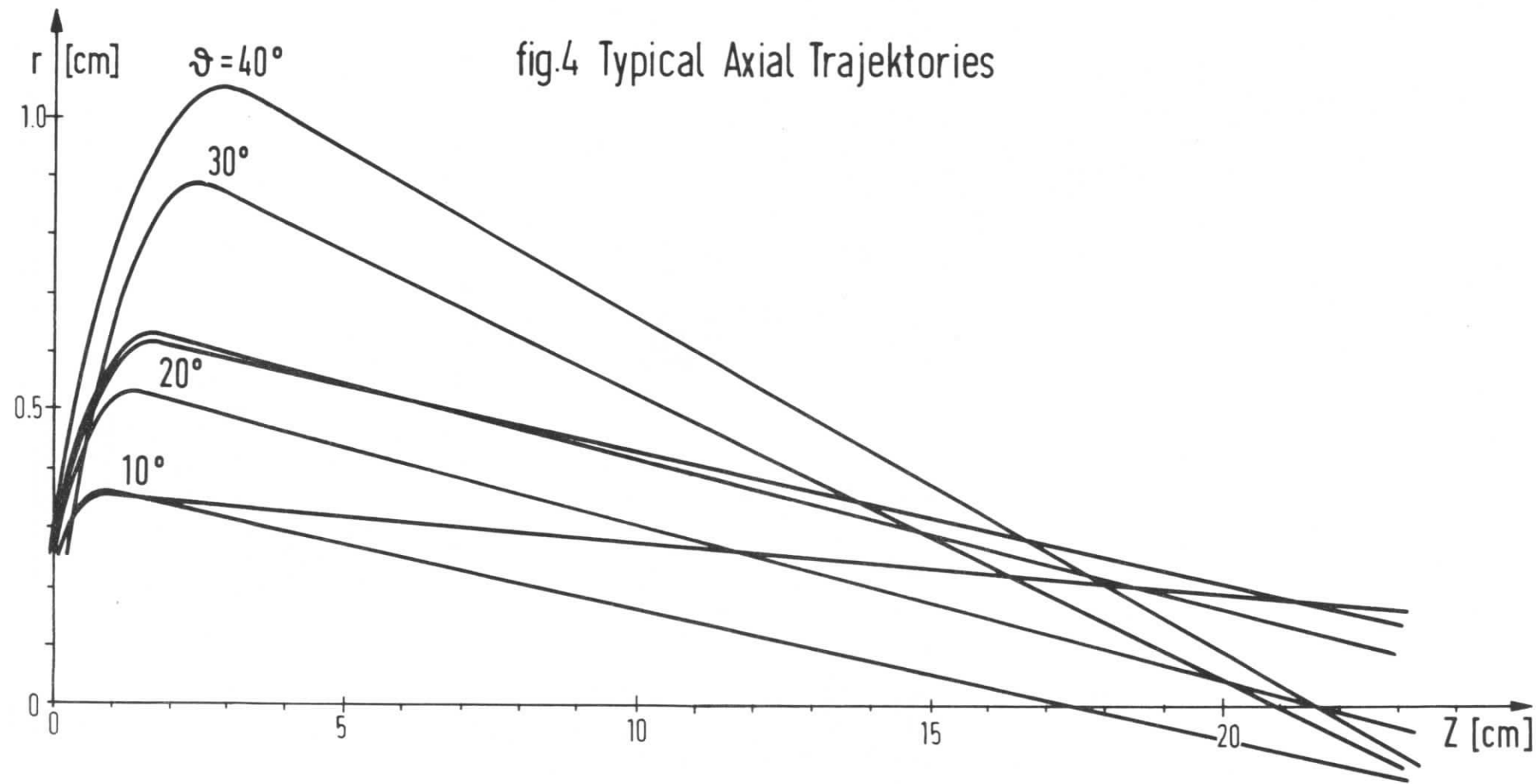


fig.5 Typical off Axis Trajectories

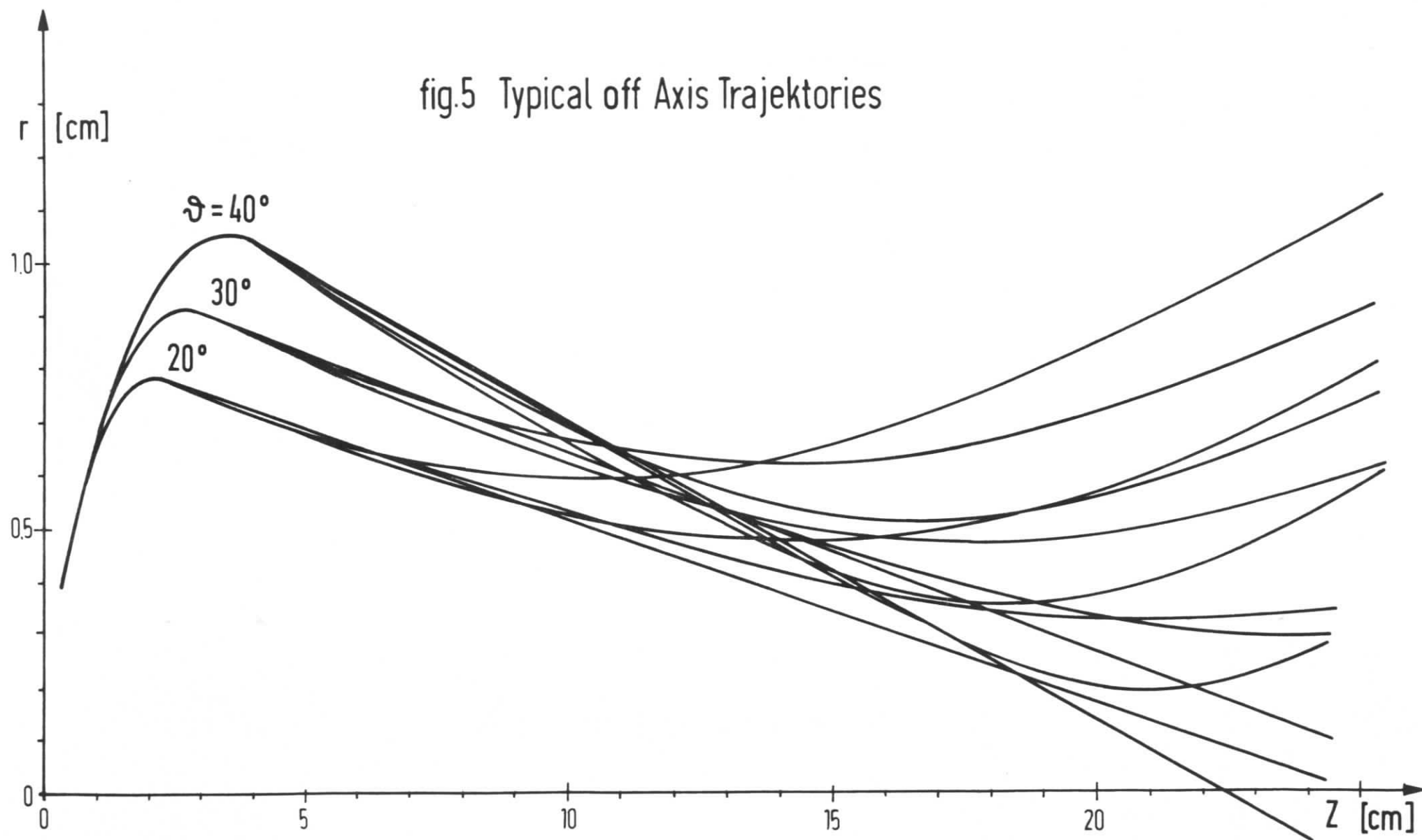
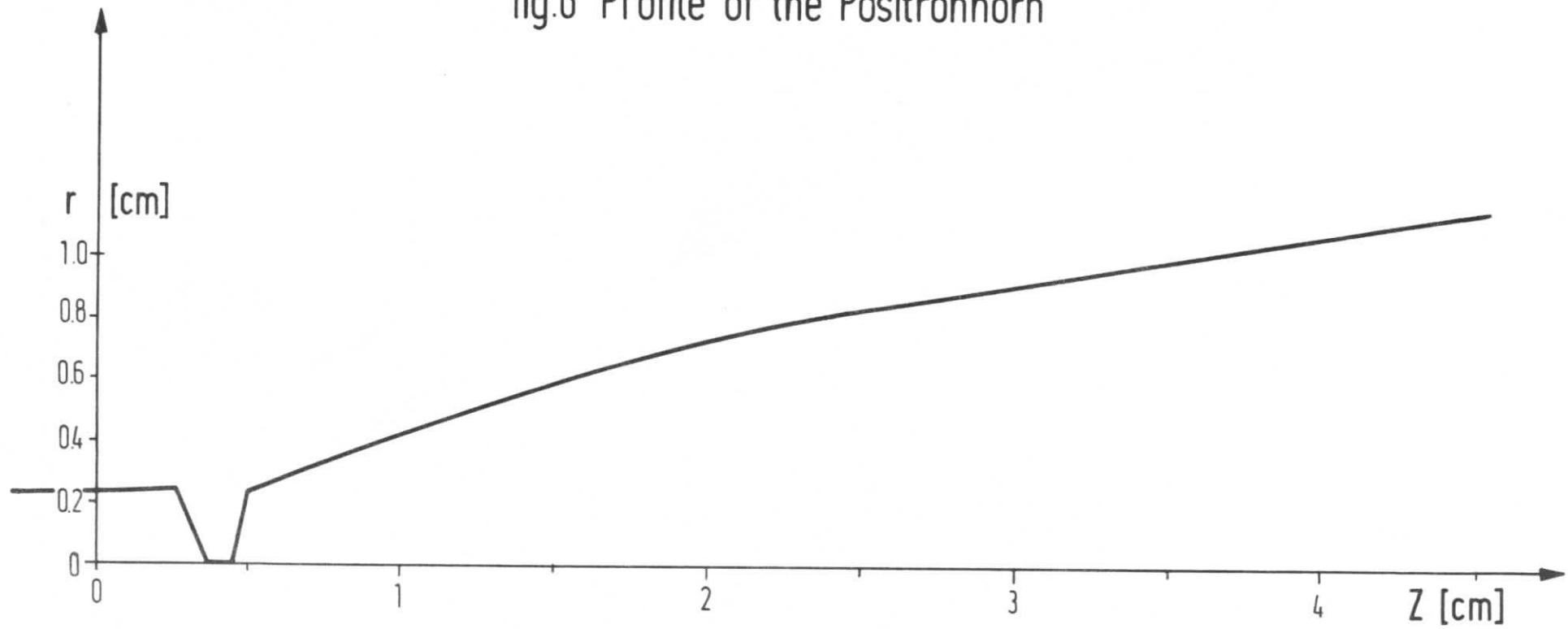


fig.6 Profile of the Positronhorn



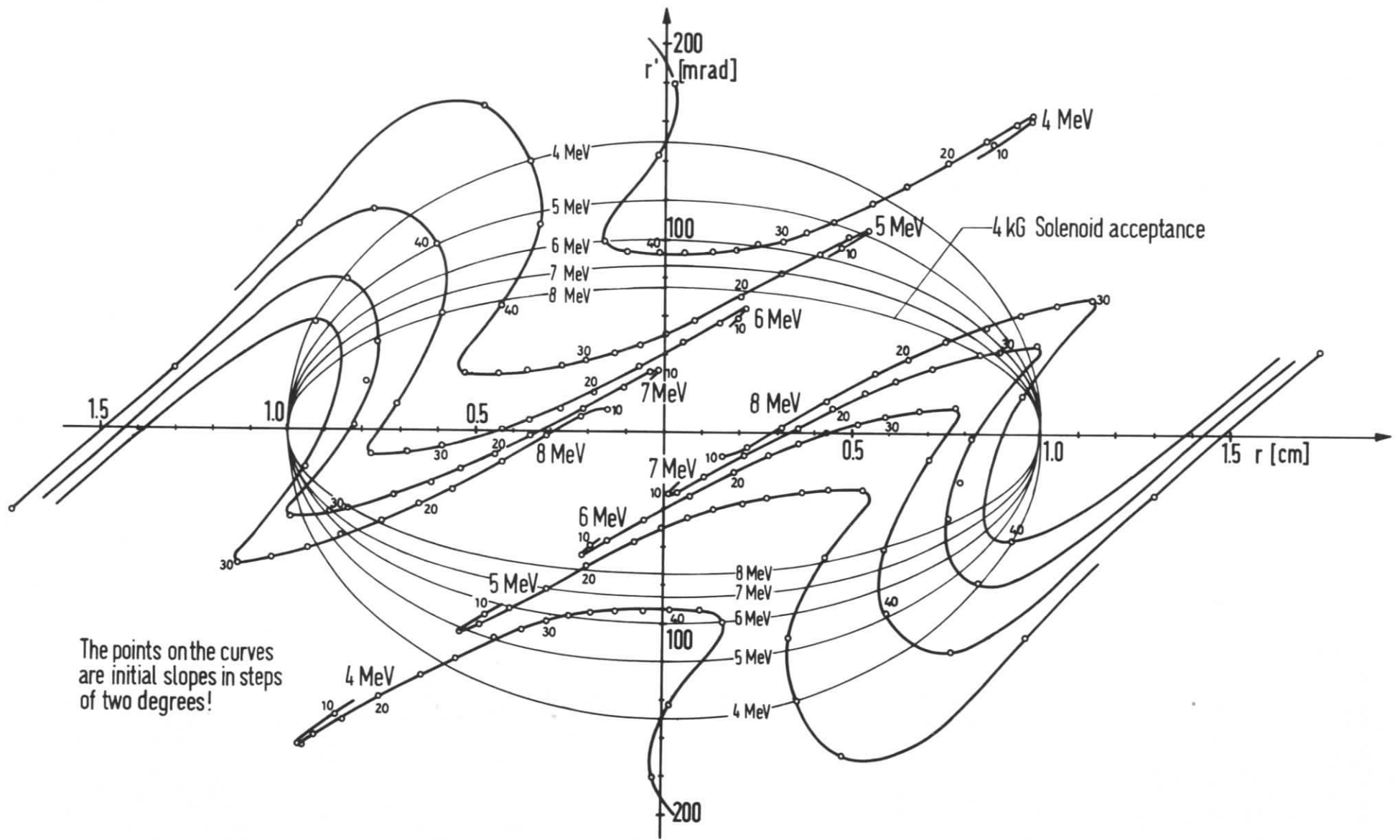


fig.7 Emittance of the Positron Horn for Various Positronenergies at  $Z=8$  cm

fig.8 Energy Distribution

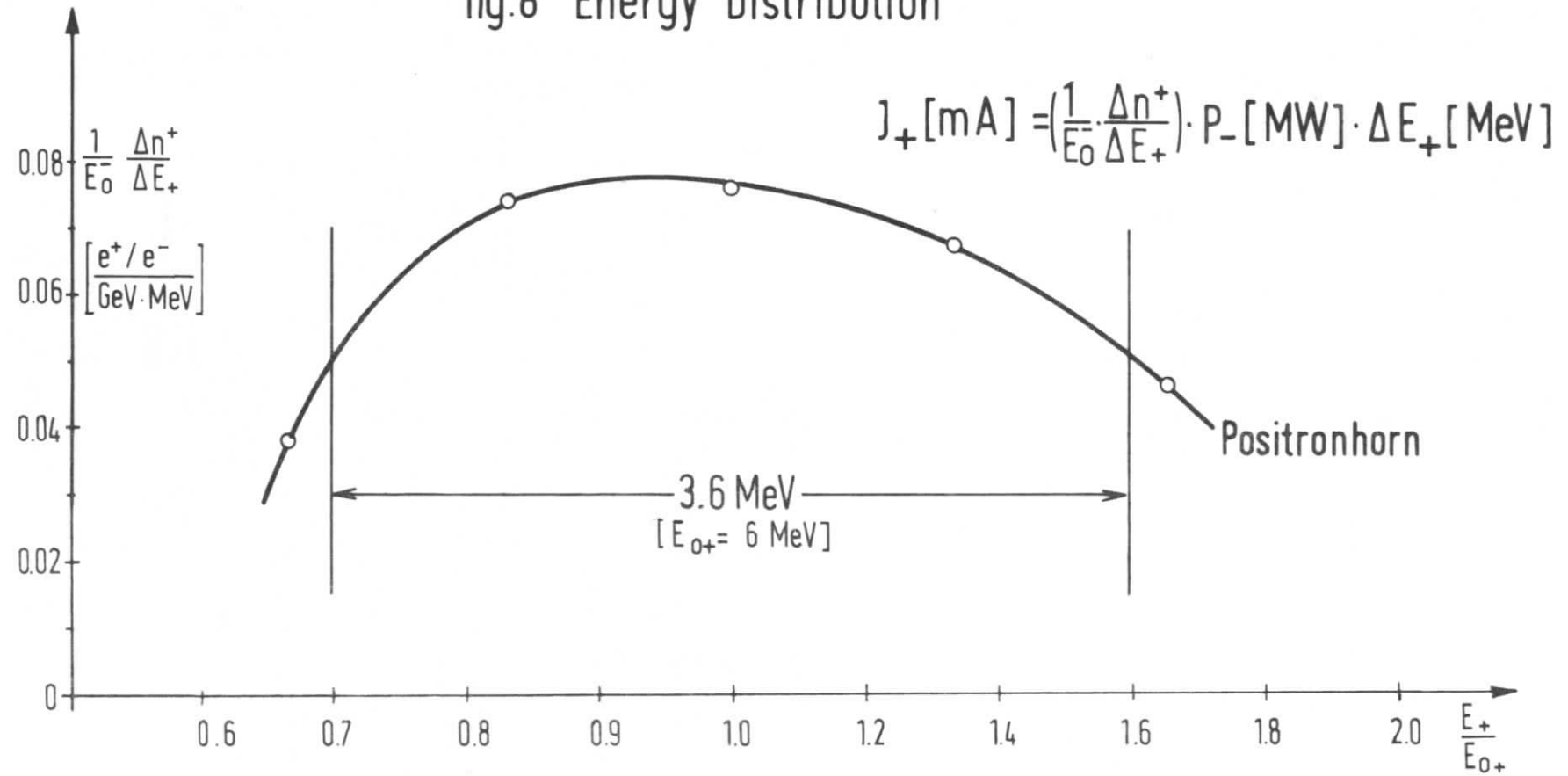


fig.8a Energy Distribution

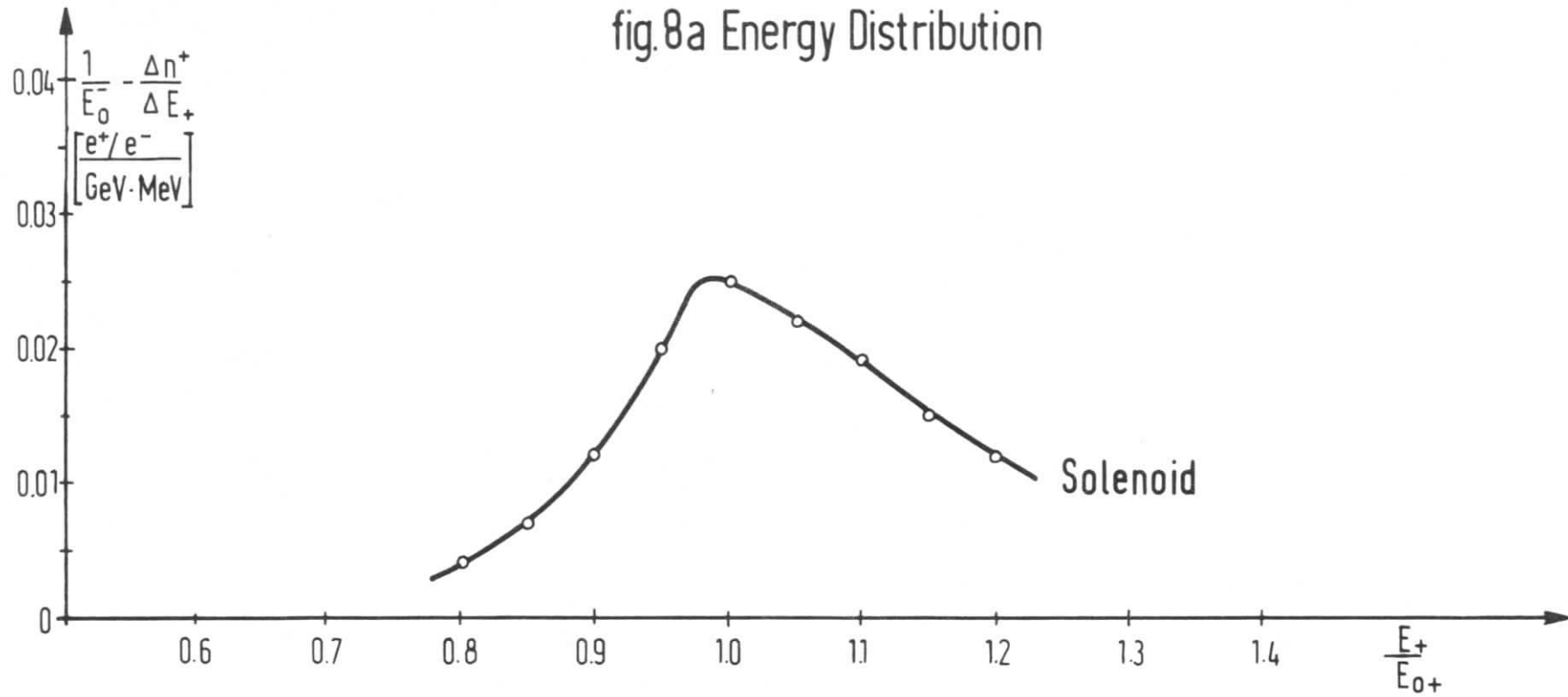


fig.9 Pathlengthdifference at  $Z = 8 \text{ cm}$

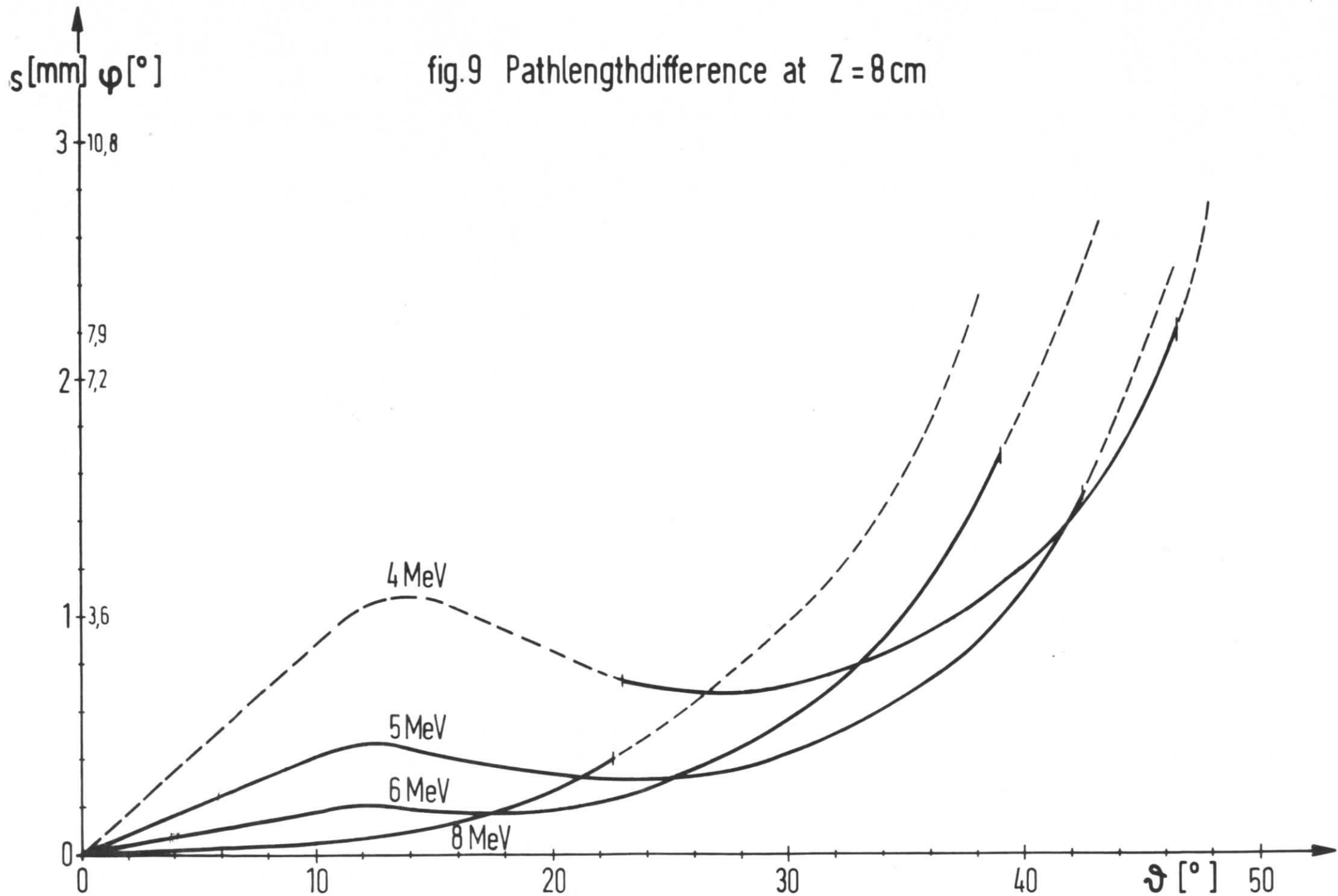


fig.10 Radial Field distribution in the Positron Horn  
8 wires

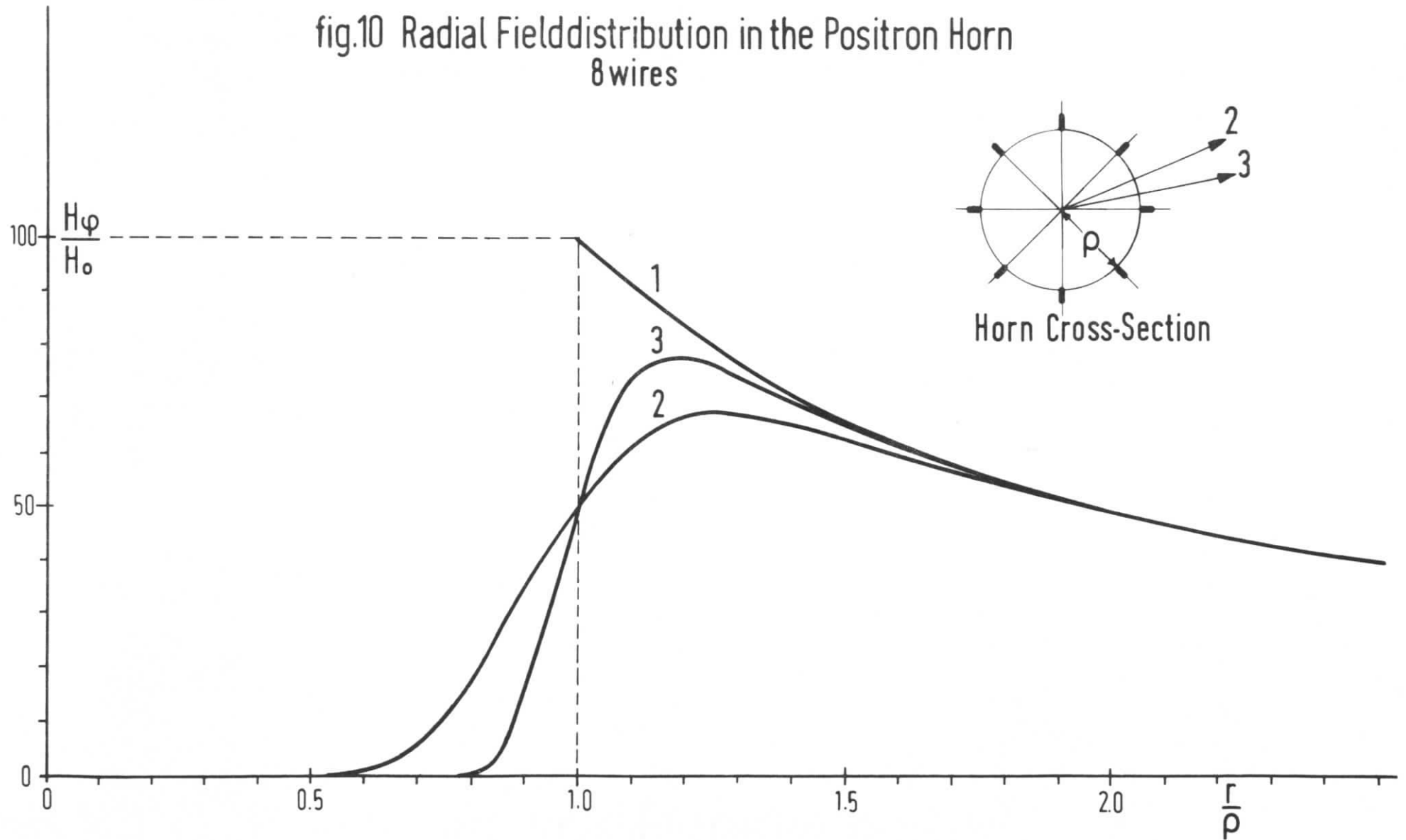
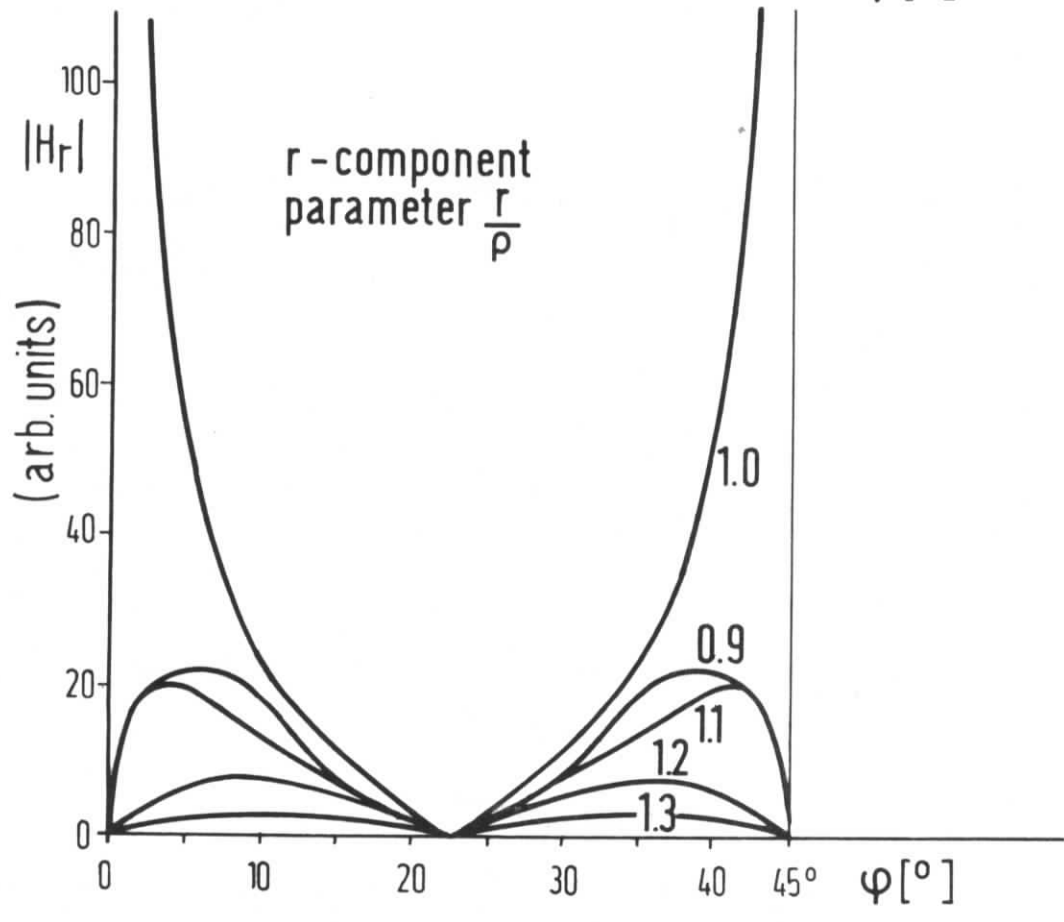
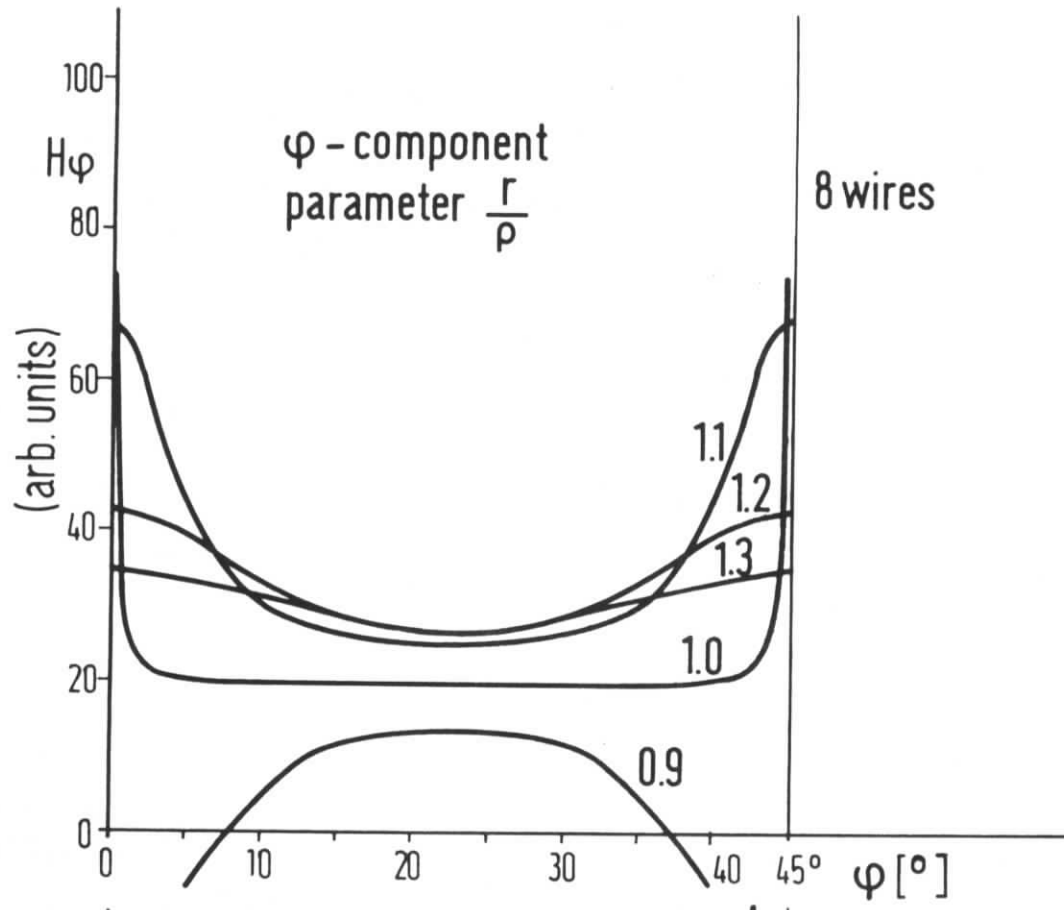


fig.11 Azimuthal Fielddistribution



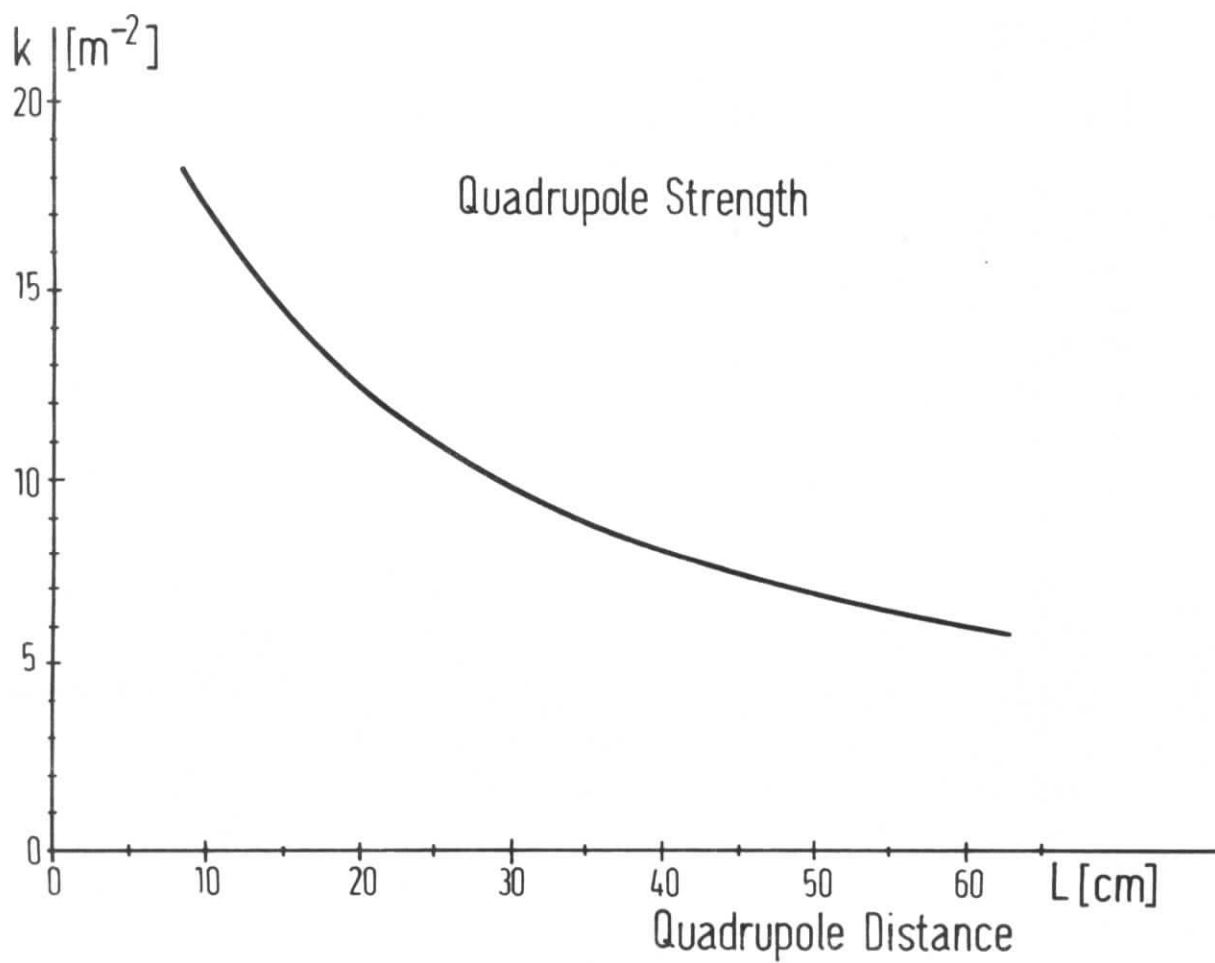
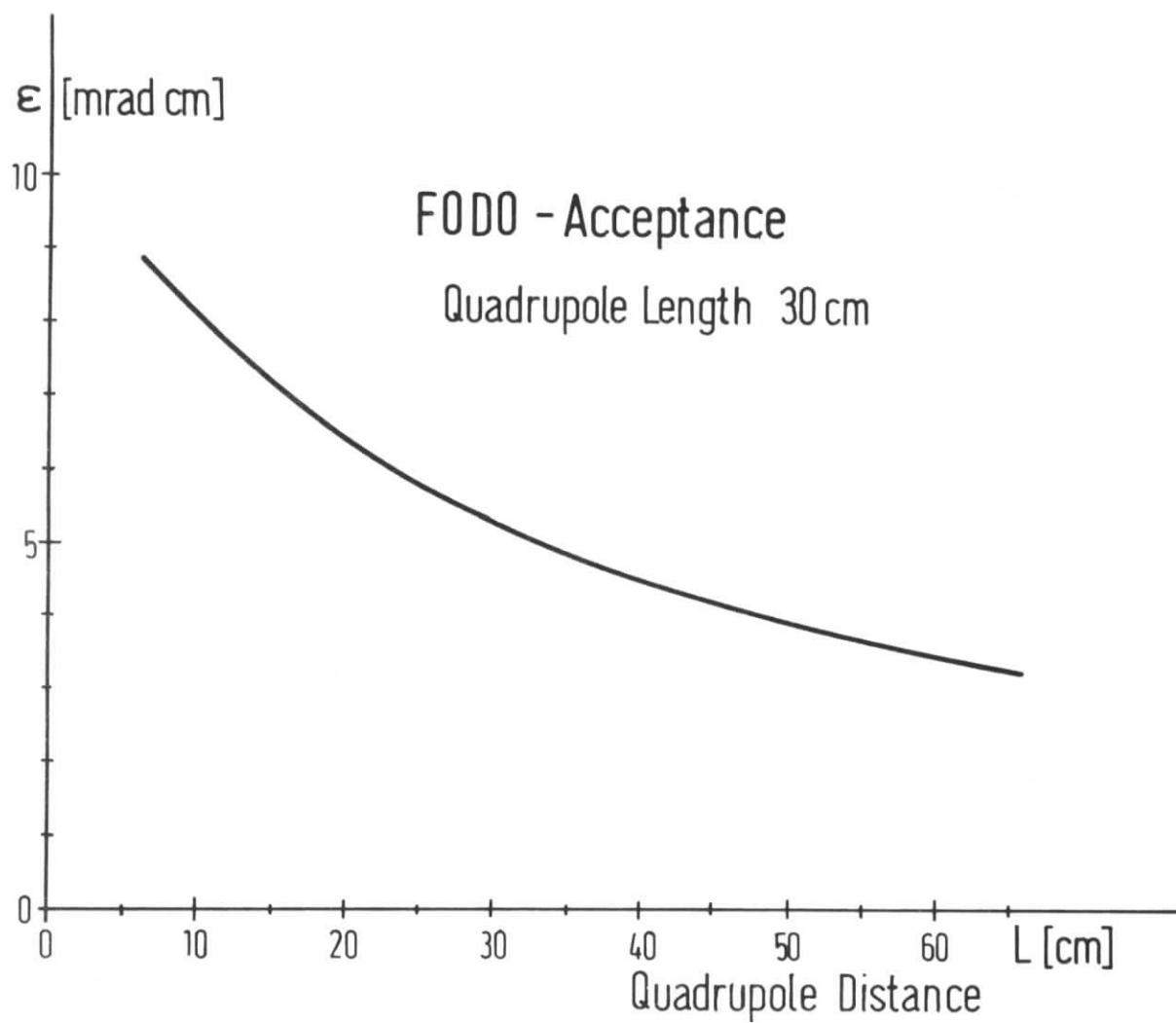


fig.12

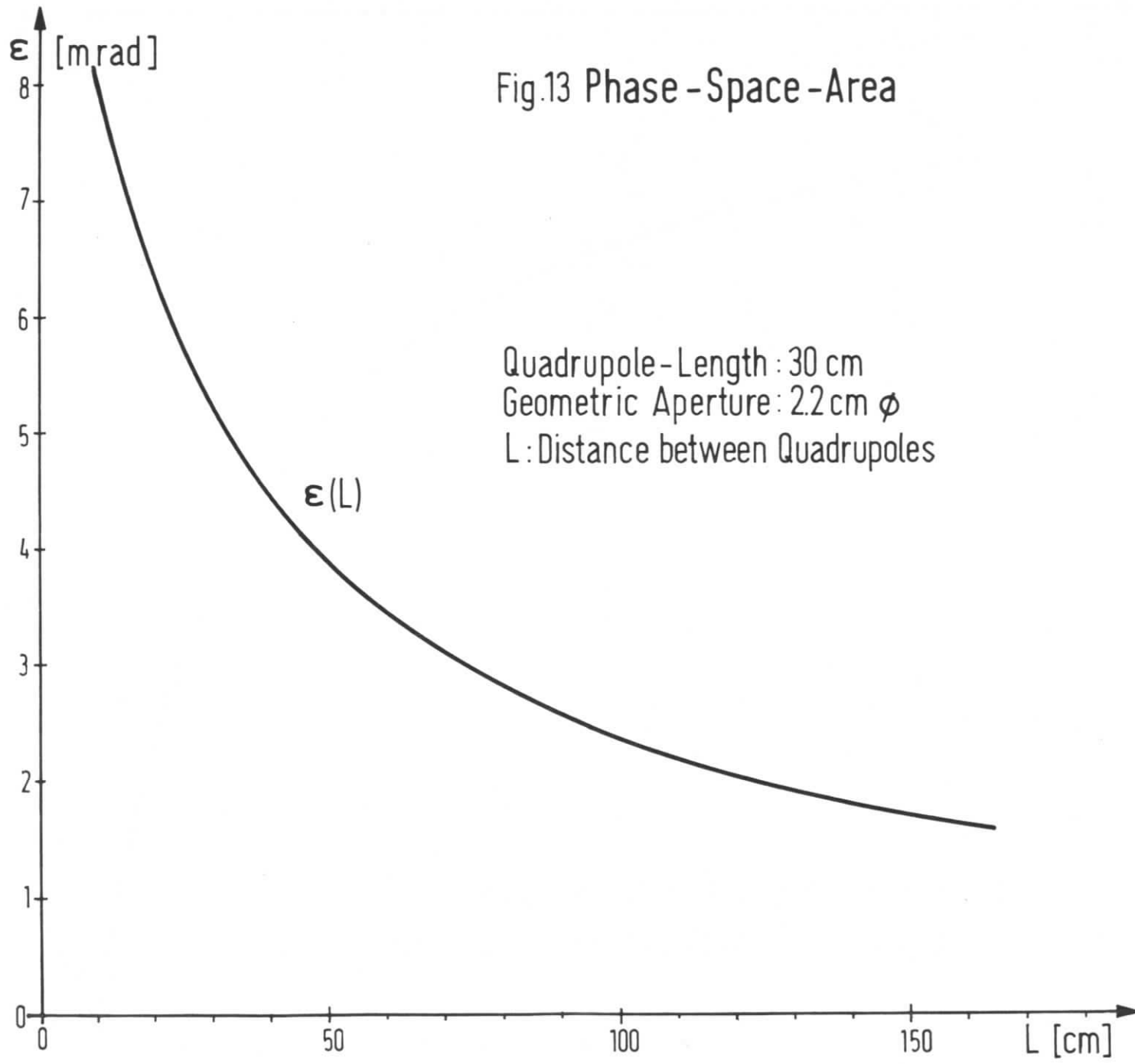


Fig.13 Phase - Space - Area

Quadrupole - Length : 30 cm  
Geometric Aperture : 2.2 cm  $\phi$   
L : Distance between Quadrupoles

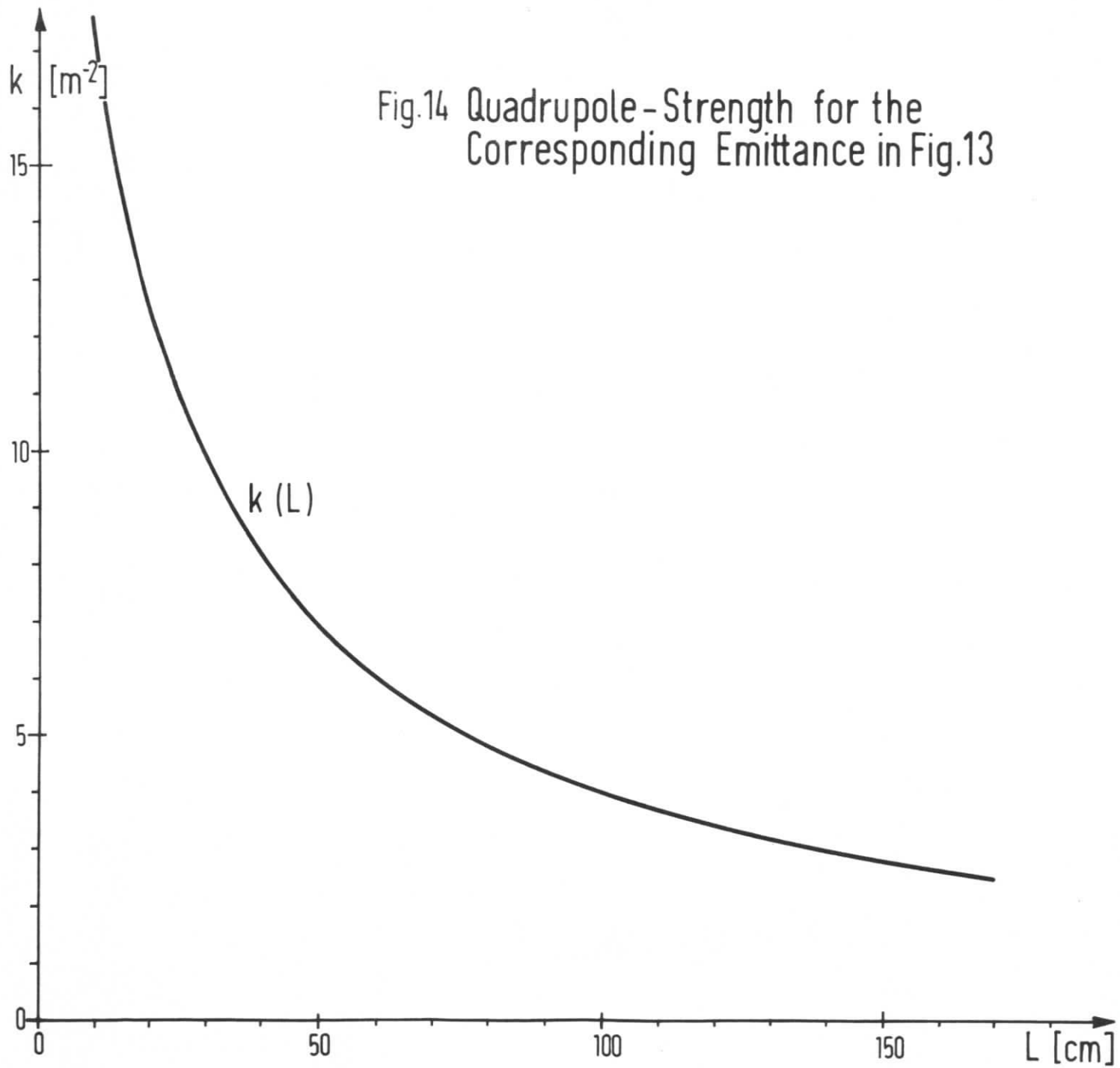


Fig.14 Quadrupole-Strength for the Corresponding Emittance in Fig.13

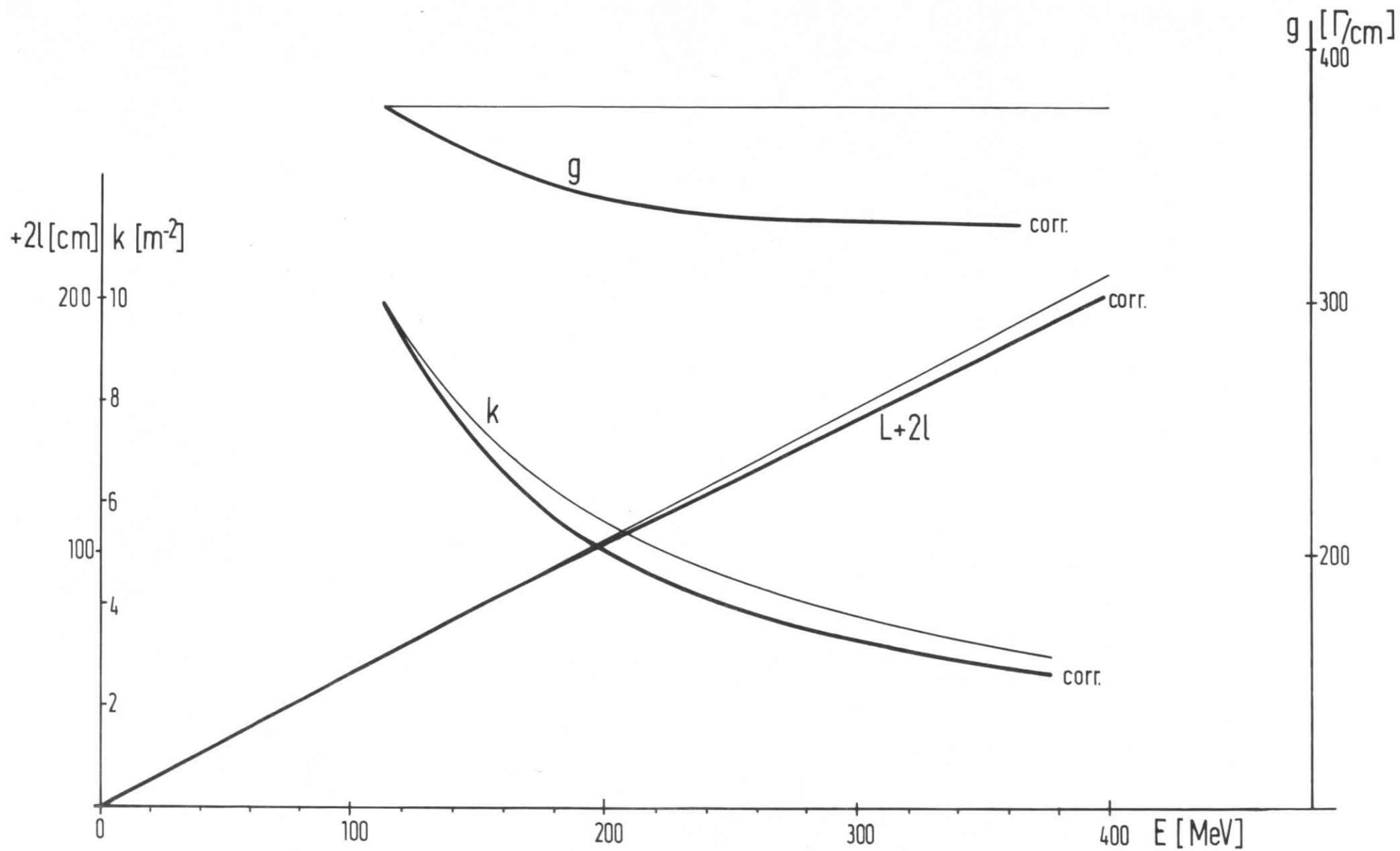


Fig.15 FODO -Channel over the Accelerator